Coherent network oscillations regulate quiescence and behavioral responsiveness in *Drosophila*

Davide Raccuglia[1,*,#], Raquel Suárez-Grimalt[1,2,*], Cedric B Brodersen[1], Jörg RP Geiger[1,2], and David Owald[1,2,3,#]

[1]Institute of Neurophysiology, Charité – Universitätsmedizin Berlin, corporate member of Freie Universität Berlin, Humboldt-Universität zu Berlin and Berlin Institute of Health, Charitéplatz 1, 10117 Berlin, Germany

[2]Einstein Center for Neurosciences Berlin, Charitéplatz 1, 10117 Berlin, Germany

[3]NeuroCure, Charité – Universitätsmedizin Berlin, corporate member of Freie Universität Berlin, Humboldt-Universität zu Berlin and Berlin Institute of Health, Charitéplatz 1, 10117 Berlin, Germany

* = shared first authors

= correspondence to DR (davide.raccuglia@charite.de) and DO (david.owald@charite.de)

Abstract

Quiescent states such as sleep restore vital physiological functions across phyla and are characterized by reduced locomotion and diminished behavioral responsiveness to external stimuli. In humans, synchronous activity across cortical networks is a hallmark of deep sleep, but how network coherence elevates arousal thresholds to maintain quiescent states remains largely unclear. Here, we build on our recent discovery of slow wave activity (SWA) mediating sleep need in the R5 ring network of *Drosophila* and investigate interactions across sleep- and arousal mediating networks. We demonstrate that information of sleep need travels across a recently described recurrent network for sleep regulation (dFSB-helicon-R5) and elicits oscillatory Ca^{2+} signatures in the presynaptic terminals of the interconnected networks. Subject to circadian modulation, the sleep need mediating circuits within this network (dFSB and R5) reciprocally promote these oscillatory signatures. Optogenetically imposing slow rhythms (1 Hz) on R5 and dFSB induces entrainable quiescent states while high-frequency stimulation of R5 (10 Hz) leads to flies losing postural control. We further discover that increased excitability in the master sleep homeostat (dFSB) likely acts as a switch that synchronizes the presynaptic electrical patterns of R5 and arousal mediating neurons (helicon) at night. Exposing the behavioral significance by optogenetically mimicking coherent activity we show that R5/helicon synchronization facilitates suppression of responsiveness to visual stimuli in sleeping flies. Moreover, neural activity in downstream head-direction neurons targeted by both helicon and R5 can be completely inhibited through activation of the R5 network. We therefore propose that sleep need mediating circuits promote coherent SWA to induce quiescent states by rhythmically associating neural networks that mediate locomotion, arousal and postural control.

Introduction

Deep sleep is characterized by a large-scale oscillatory coherence across cortical networks of the human brain (Buzsaki and Draguhn, 2004). As cortical networks synchronize during sleep, slow-wave activity (SWA) becomes apparent during local field potential (LFP) measurements such as electroencephalograms (EEGs), which are generally used in humans to assess different brain states during wakefulness and sleep (Adamantidis et al., 2019). Network coherence during sleep is hereby proposed to be orchestrated by reciprocal interactions between cortical and thalamic oscillations (Crunelli and Hughes, 2010). The mammalian thalamus relays sensory and motor information and its interaction with the cortex is therefore crucial for inducing and maintaining sleep, as well as regulating behavioral responsiveness to sensory stimuli (Andrillon and Kouider, 2020; Gent et al., 2018). It is thus of general interest, how interactions between networks can underly network coherence to promote sleep and downregulate responsiveness to allocentric or world-centered, sensory cues to enter an internal, more egocentric state, while maintaining the ability to 'break' this state through salient sensory stimuli.

Recent evidence indicates that neural networks can display a sleep-like state independent of the rest of the brain, a phenomenon described as 'local sleep' (Krueger et al., 2019; Vyazovskiy et al., 2011). Local sleep occurs when neural networks have been excessively engaged in sensory processing and are associated with cognitive deficits in mammals (Quercia et al., 2018; Vyazovskiy et al., 2011). Therefore, electrical synchronization resulting in SWA are network-independent markers of sleep need and might represent a fundamental neural principle for shutting down sensory processing to undergo synaptic plasticity. Indeed, this notion is supported by the observation that the ability to generate SWA is maintained in isolated cortical and thalamic networks (Sanchez-Vives and McCormick, 2000). As oscillatory coherence in intact brains results from a complex interplay between networks, it is difficult to assess how these interactions contribute to the emergence of compound SWA. Therefore, several aspects regarding the fundamental and potentially evolutionarily conserved interactions of networks and the functional relevance of SWA in regulating quiescent states remain unclear.

SWA associated with sleep and sleep need has been observed in mammals (Siclari and Tononi, 2017), birds (Low et al., 2008), reptiles (Shein-Idelson et al., 2016), fish (Leung et al., 2019), crabs (Ramon et al., 2004) and recently in the vinegar fly *Drosophila melanogaster* (Raccuglia et al., 2019). In *Drosophila*, sleep is primarily defined by prolonged inactivity (≥5 min), reduced arousability and homeostatic regulation, as prolonged wakefulness leads to deeper and prolonged sleep (Shaw et al., 2000). Fine-architectures of sleep states are phenotypically conserved from flies to humans and also associated with an increase in oscillatory activity, as measured with LFP recordings in the central brain of *Drosophila* (Yap et al., 2017). Recent years have established that sleep in *Drosophila* is regulated by the higher sensory processing centers of the central complex and the mushroom bodies (Donlea, 2019; Sitaraman et al., 2015). At the level of the central complex it has become clear that the dorsal fan-shaped body (dFSB) encodes a sleep switch (Donlea et al., 2009; Pimentel et al., 2016) that interacts with ExR1/helicon cells, which process visual information and gate locomotion, positioning this network as an ideal candidate for balancing arousal and sleep (Donlea et al., 2018). Moreover, helicon cells interact with the R5 network, which based on its connectivity likely can engage in both navigation and sleep regulation (Flores-Valle et al., 2021). We recently discovered that in the R5 circuit, network-specific synchronization generating compound SWA arises over the day to integrate circadian and homeostatic sleep drive, tilting flies towards sleep or maintaining it to ensure adequate sleep quality (Raccuglia et al., 2019). Similar to thalamocortical circuits, the current brain state and the ability to generate SWA is maintained *ex vivo* (Liu et al., 2016; Raccuglia et al., 2019; Sanchez-Vives and McCormick, 2000), enabling us to study activity patterns and network interactions in a sleepy brain.

Here, we investigate how the functional components of reciprocally connected networks (dFSB-helicon-R5) interact to regulate quiescence via SWA. Using a strategy that combines genetically-encoded voltage and Ca^{2+} sensors with optogenetics, we discovered that the networks within this circuitry facilitate each other in generating compound SWA. Behavioral analyses show that optogenetically imposing 1 Hz rhythmic activity on dFSB and R5 independently puts flies in a quiescent state, reducing locomotor activity to a degree similar to that observed in sleep deprived flies. In contrast, optogenetic activation of the helicon cells increased locomotion. We discovered that, at

night, helicon and R5 synchronize their electrical SWA, which reduces behavioral responsiveness to light and can effectively function as a sensory gate that aids maintaining sleep to ensure adequate sleep quality. Head direction neurons (EPG) which are part of a navigational system are downstream targets of helicon and R5 and show nighttime specific reduction in activity, which can be partially mimicked by rhythmically stimulating R5 during the day. We therefore propose that R5 shuts off arousal-mediated action of helicon by associating EPG neurons to its rhythmic night pattern, inducing a quiescent state that switches the animal from an allocentric-like to a more egocentric-like mode.

Results

Electrical slow-wave activity in the master sleep homeostat in *Drosophila*

In the human brain, sleep-related slow-wave oscillations (0.5-4 Hz) typically spread across several brain regions during sleep or mounting tiredness (Adamantidis et al., 2019). We recently identified rhythmic slow-wave activity local to the R5 network in *Drosophila* (Raccuglia et al., 2019). Emergence of network-specific slow-waves correlated to undisrupted sleep and resulted from single unit synchronizations. We started this study by asking whether sleep-relevant SWA was constrained to R5 neurons or a typical hallmark of sleep-regulating centers.

To test this, we turned to the dFSB network that comprises neurons that integrate and execute sleep drive (Donlea et al., 2014). Expression of the voltage indicator (GEVI) ArcLight (Cao et al., 2013; Raccuglia et al., 2016) was genetically targeted to the dFSB allowing for simultaneous imaging of several individual cell bodies or compound electrical activity in a whole brain explant preparation **(Fig. 1A-F)**. Multi-cellular recordings revealed low overall activity of dFSB neurons in the morning hours **(Fig. 1B)**. General activity markedly increased in the evening and power analysis revealed an activity peak around 1 Hz **(Fig. 1B, C)**. However, unlike what we previously observed for the R5 network (Raccuglia et al., 2019), activity was only loosely correlated between the single units regardless of whether measured during the morning or the night hours **(Fig. 1D)**. Nonetheless, we observed an increase in slow-wave power (0.5-1.5 Hz) when measuring the presynaptic compound signal, which represents the coherent activity of

the whole dFSB network (comparable to local field potentials) **(Fig. 1E, F)**. While compound activity of the dFSB was somewhat reminiscent of the activity patterns previously observed in the R5 network (Raccuglia et al., 2019), the underlying mechanism in the dFSB appeared to differ from that of R5.

To investigate the temporal relationship between R5 and dFSB compound electrical patterns at night, we performed dual color voltage imaging experiments by simultaneously expressing the green voltage indicator ArcLight and the red voltage indicator Varnam (Kannan et al., 2018) in R5 and dFSB, respectively **(Fig. 1G, H)**. A cross correlation analysis demonstrated that the electrical patterns of the two neural populations were largely overlapping **(Fig. 1I)** while they slightly differed in their peak frequencies **(Fig. 1J)**. Therefore, both dFSB and R5 networks exhibit oscillatory activity and are likely interconnected, as previously reported R5 to dFSB interactions with respect to mediating sleep drive would suggest (Liu et al., 2016). Similar to the thalamocortical system, reciprocal interactions between R5 and dFSB could induce and maintain sleep-relevant SWA, pinpointing to a universal neural mechanism of sleep regulation.

Reciprocal interactions between neural circuits promoting sleep

To directly test for functional interactions of network activity patterns, we first asked whether R5 activation could induce dFSB oscillations **(Fig. 2A-C)**. We suppressed spontaneous network activity using a previously established high Mg^{2+} extracellular saline (Raccuglia et al., 2019) and optogenetically stimulated R5 neurons using the red-light shifted channelrhodopsin CsChrimson (Klapoetke et al., 2014) while monitoring intracellular Ca^{2+} in presynaptic terminals of the dFSB **(Fig. 2A)**. As presynaptic Ca^{2+} is an adequate proxy for determining the bandwidth of synaptic output, we here focused on compound Ca^{2+} oscillations of the sleep drive-mediating neural circuits. Optogenetic stimulation of R5 reliably induced or amplified presynaptic SWA in the dFSB **(Fig. 2B)**. This effect was only statistically significant after terminating optogenetic activation **(Fig. 2C)**, indicating that activation of R5 neurons can lead to longer lasting physiological changes in the dFSB. This finding is in accordance with the observation that sleep need increases mainly after thermogenetic activation of R5 and moreover requires synaptic output from the dFSB (Liu et al., 2016). Interestingly, the power of the observed SWA in

dFSB neurons was more pronounced during the subjective night **(Fig. 2C)**, demonstrating the influence of the circadian clock on interactions between sleep drive mediating neural circuits.

To investigate a potential reciprocal connection between the dFSB and R5, we next optogenetically activated the dFSB and recorded presynaptic Ca^{2+} activity in R5 **(Fig. 2D)**. Optogenetic activation of the dFSB did not elicit Ca^{2+} oscillations during the day **(Fig. 2E),** but elicited pronounced oscillations during the stimulation at nighttime **(Fig. 2F)**. Moreover, in about 50% of the cases, R5 SWA persisted even after optogenetic activation ceased (data not shown), suggesting that increased excitability of the dFSB entrains R5 oscillations and might thus affect sleep need on a longer time scale.

To directly test whether the increased excitability of the dFSB at night drive SWA in R5, we optogenetically inhibited the dFSB using the light-gated chloride channel GtACR (Mohammad et al., 2017) **(Fig. 2G)**. Here, to access the potential effect of inhibition, we used a low Mg^{2+} extracellular saline that does not suppress spontaneous activity (Raccuglia et al., 2019). Indeed, activating GtACR in the dFSB reduced oscillatory power of the R5 network **(Fig. 2H, I)**, further supporting the notion that sleep need mediating SWA in R5 neurons is facilitated by increased excitability within the sleep-executing neurons of the dFSB. This effect was not observable in controls not expressing GtACR **(Fig. 2H, I)**. However, often during optogenetic inhibition, R5 SWA quickly recovered (data not shown), suggesting that R5 SWA is stabilized either through other synaptic inputs (such as TuBu) (Lamaze et al., 2018; Raccuglia et al., 2019) or through cell-autonomous promotion of SWA. Short-term optogenetic inhibition of the dFSB confirmed a transient reduction of presynaptic Ca^{2+} in R5 and moreover displayed a post-stimulus increase in R5 neurons **(Fig. S1)**.

Our data so far suggest that reciprocal interactions between network activity in the dFSB and R5 together with coincident information about the time of day modulate sleep drive mediating SWA. Oscillatory frequencies observed after activating specific networks slightly vary from spontaneously occurring SWA at night, suggesting that compound SWA in the *Drosophila* brain is finetuned by an interplay of several networks. After demonstrating that prominent sleep-regulating structures exhibit similar, but not

identical mutually interactive oscillations at night, we next addressed to what extent the temporal structure of network activity was relevant for behavior.

Neural circuits mediating sleep drive acutely control locomotor behavior

Activation of both R5 and dFSB has profound impact on fly sleep behavior (Liu et al., 2016; Pimentel et al., 2016; Raccuglia et al., 2019). In fact, tonic artificial activation of the dFSB reduces behavioral responsiveness to external stimuli and leads to a quick transition to sleep (Troup et al., 2018).

We devised a paradigm for tracking freely moving flies in a small circular arena while performing temporally fine-tuned optogenetic activation experiments **(Fig. 3A)**. To demonstrate that the locomotion of flies in this arena is subject to their internal sleep need, we compared locomotor activity of rested and sleep deprived flies **(Fig. 3B)**. As expected, the mean velocity of sleep deprived flies was significantly reduced compared to rested flies **(Fig. 3B).** Moreover, about 56% of sleep deprived flies were immobile for 5 min, which represents the generally accepted criteria for sleep (Shaw et al., 2000), indeed demonstrating that the flies' locomotor activity in the arena is subject to their internal sleep need.

We first asked whether 1 Hz optogenetic activation of the dFSB could acutely regulate locomotor activity in rested flies **(Fig. 3C)**. Importantly, optogenetic activation of dFSB neurons at 1 Hz had previously been shown to reliably promote the naturally occurring oscillatory pattern in single dFSB neurons (Troup et al., 2018). To be more sensitive to the induction of potential sleep states, we performed these experiments during the subjective day (ZT 1-10). 1 Hz stimulation of the dFSB decreased the walking velocity as well as the time spent walking **(Fig. 3D-E and S2A)**, thus drastically reducing locomotor activity which is in accordance with the strongly sleep-promoting function of the dFSB. Of note, during optogenetic activation flies displayed short bouts of walking and movement of the wings and caudal body parts. Of note, during optogenetic activation flies displayed short bouts of walking and movement of the wings and caudal body parts, which is in line with previous reports showing that during dFSB activation, flies are still capable of walking and reacting to external stimuli (Tainton-Heap et al., 2021; Troup et al., 2018). Interestingly, we found that flies only fully recovered to baseline locomotor activity 10 min after activation offset. To exclude the possibility that the observed

behavior was a visually triggered response to pulsed light, we evaluated the effect of the optogenetic protocol on the locomotion of flies carrying only the UAS-CsChrimson transgene. We found that pulsed light slightly reduced locomotor activity **(Fig. 3D, E, compare to 3I, J)**, indicating that rested flies become aroused by red light. However, inhibition of locomotor activity through dFSB activation was considerably stronger **(Fig. 3E, compare to 3J).** To test whether inhibition of locomotion was frequency-specific, we next stimulated dFSB neurons at 10 Hz. We observed locomotor phenotypes comparable to 1 Hz stimulation, indicating that stimulation frequency was not crucial for the observed behavior **(Fig. 3F, S2B).**

We next tested whether, similar to the dFSB, acute rhythmic optogenetic activation of R5 would also affect locomotion activity in rested flies (**Fig. 3G**). Activating R5 at 1 Hz, flies significantly reduced locomotion similar to what we observed when stimulating the dFSB (**Fig. 3H-I**). During optogenetic R5 stimulation flies displayed short walking bouts as well as frequent grooming. Unlike what was observed in the dFSB experiments, locomotion recovered much slower after stimulation offset, not reverting to normal for the following 10 min. This is in line with R5 activity entraining the involved neural circuits to prepare flies for sleep and promote more consolidated sleep phases (Raccuglia et al., 2019). While walking velocity was only slightly affected, reduced locomotion was mainly due to a reduction in total time spent walking **(Fig. 3I and S2C).** We therefore conclude that flies were not impaired in their ability to walk. However, we also examined the flies' behavioral responsiveness to an arousing air-puff during 1 Hz R5 stimulation and found that flies indeed reacted to the stimulus by increasing their walking velocity **(Fig. 3J)**. Together, these results suggest that R5 activation at 1 Hz reduces locomotor activity while leaving the ability to walk intact. Reduction of locomotor activity was not observed in genetic controls and flies lacking the obligatory CsChrimson cofactor all-*trans* retinal **(Fig. S2C)**. Of note, inhibiting locomotion is not general to ring neurons, as it was not observed when activating R3 neurons at 1 Hz **(Fig. S2E)**.

Strikingly, stimulating R5 at 10 Hz rendered flies immobile and they often lost postural control during optogenetic activation, sometimes lasting for 5 min post-stimulation **(Fig. S2D)**. Stimulating R5 neurons at 0.1 Hz did not lead to a measurable impact on the flies' behavior **(Fig. S2D)**. Therefore, contrary to the dFSB, the activation frequency mattered

for the R5 network **(Fig. 3K)**, potentially placing the R5 network as instructive for an ongoing brain state (such as sleep). While the slow oscillations observed in R5 might allow the flies to maintain natural body posture during quiescence it is possible that over-stimulating R5 neurons at 10 Hz overrules downstream effectors involved in standing upright.

Importantly, 1 Hz R5 activation induced a quiescent state characterized by reduced locomotor activity and frequent grooming, which has been associated with periods of rest (Qiao et al., 2018). In line with this, 1 Hz optogenetic activation of R5 in rested flies reduced locomotor activity to the level of awake sleep deprived flies **(Fig. 3L)**, suggesting that R5 activation at this frequency increases sleep need in awake animals.

Taken together, these data indicate that acute activation of neural circuits mediating sleep drive at a frequency band of sleep-relevant SWA at night controls locomotor behavior, inducing a quiescent state characterized by reduced locomotion.

Oscillatory signatures in locomotion-gating helicon cells

Our data demonstrate mutual interactions between the dFSB and R5 networks and indicate that these structures are functional analogs at the behavioral level. Using the recently published hemiconnectome of *Drosophila* (Scheffer et al., 2020), we next investigated putative neural connections between the dFSB and R5 and found no direct synaptic connections **(Fig. 4A)**. Instead, our analysis revealed that R5 neurons are highly interconnected with the previously identified helicon network (Donlea et al., 2018). These four neurons make reciprocal all-to-all synaptic connections with R5 **(Fig. S3A)** that represent about 24% of R5 input and output connections **(Fig. 4A)**. Similarly, R5 neurons are one of the main pre- and postsynaptic partners of helicon cells **(Fig. S3B)**. Consistent with previous observations showing that dFSB neurons inhibit visually evoked responses in helicon cells (Donlea et al., 2018), we found that helicon cells make reciprocal connections to the dFSB **(Fig. S3C)** (Hulse et al., 2021). Our analysis further indicates that, as previously suggested, recurrent connections from helicon cells could constitute a main route to relay neural information between the dFSB and R5 networks and vice versa **(Fig. 4B and S3D)**.

At the behavioral level, helicon cells have been shown to gate visually evoked locomotion (Donlea et al., 2018). We next asked whether imposing 1 Hz activity patterns on helicon cells would be sufficient to modulate locomotor activity in rested flies **(Fig. 4C)**. In line with previous results, flies increased walking velocity and spent more time walking **(Fig. 4D, E and S3E**), essentially increasing locomotor activity during optogenetic stimulation. This locomotion-promoting effect was not observed in genetic control flies carrying the UAS-CsChrimson transgene **(Fig. 4D, E).** Contrary to dFSB and R5 activation, helicon stimulation did not affect locomotor activity after activation offset. Activating helicon cells at 10 Hz led to a comparable effect on locomotor activity, suggesting that the frequency of activation is not a critical factor for gating locomotion **(Fig. 4F)**.

Interestingly, at the single cell level, it was recently shown that the dFSB hyperpolarizes helicon cells to inhibit visual processing (Donlea et al., 2018). To investigate whether these changes in membrane potential are subject to diurnal modulation, we measured basal fluorescence levels using the voltage indicator ArcLight at the level of the cell bodies to approximate changes in resting membrane potential during morning and evening hours. Indeed, increased levels of fluorescence indicate that helicon cell membrane potential was more hyperpolarized at night (data not shown) relative to the morning hours, indicating that increased excitability of the dFSB reduces excitability in the helicon cells as a function of the time of the day.

To test whether, similar to the R5 network, the helicon network might integrate sleep drive at the level of presynaptic Ca^{2+} (Liu et al., 2016), we used prolonged activation of ectopically expressed ATP receptors (Claridge-Chang et al., 2009) in the dFSB **(Fig. 4G)**. We found that helicon cells strongly increased presynaptic Ca^{2+}-levels in the ring **(Fig. 4H, J)** and moreover observed a transient increase in oscillatory activity **(Fig. 4H-K)** that was mostly associated with a surge in presynaptic Ca^{2+}-levels (data not shown). However, in comparison with spontaneously occurring activity in dFSB and R5, the observed helicon activity was mainly in a frequency range between 0-0.5 Hz **(Fig. 4I)**. Our findings suggest that similar to R5 neurons, sleep need is encoded in elevated presynaptic Ca^{2+}-levels (Liu et al., 2016) and increased oscillatory activity (Raccuglia et al., 2019) in helicon cells. To test whether activation of helicon cells can directly induce sleep regulating compound oscillations in R5 presynaptic terminals we further

investigated the physiological interactions between the helicon and R5 networks. We first attempted optogenetic stimulation of helicon cells, but failed to induce oscillations in R5 presynaptic terminals (data not shown). However, similar to previously reported increase in EPSPs induced at the level of single R5 cell bodies (Donlea et al., 2018) some recordings showed minor compound Ca^{2+} activity at the level of R5 presynaptic terminals (data not shown). Guided by the observation that prolonged activation of helicon cells increases sleep need (Donlea et al., 2018), we next tested whether prolonged activation of helicon cells via ectopically expressed ATP receptors can increase R5 compound oscillations **(Fig. 4L)**. In fact, we found that strong and prolonged activation of the helicon cells can potentiate R5 slow wave power at the level of compound presynaptic activity **(Fig. 4M, N)**. However, as observed in the helicon cells, the frequency range of the induced SWA was slower in comparison to spontaneously occurring R5 SWA, suggesting that different neural inputs need to come together to modulate R5 SWA in a sleepy brain (see Discussion).

Network coherence regulates behavioral responsiveness

So far, we have demonstrated that prolonged activation of the master sleep homeostat in *Drosophila* induced oscillatory signatures in the locomotion gating helicon network which, in turn, can potentiate sleep regulating oscillatory activity in R5. Since helicon cells and R5 neurons seem to play a role in both visually guided navigation and mediating sleep need, it is likely that temporal interactions between the activity patterns of these circuits regulate locomotor activity during wake and sleep. To investigate this relationship, we simultaneously recorded the electrical compound activity at their overlapping presynaptic sites by performing dual color voltage imaging experiments expressing the green voltage indicator ArcLight in R5 and the red voltage indicator Varnam in helicon **(Fig. 5A)**. We confirmed that in both R5 and helicon oscillatory power (0.5-1.5 Hz) is increased at night compared to the subjective morning **(Fig. 5B, C)**. Most interestingly, correlation between the electrical patterns of these neural populations was significantly increased at night **(Fig. 5D),** suggesting that coherence between these neural populations might play a role in mediating sleep drive and potentially in maintaining sleep.

In mammals, synchronization of SWA between neural circuits occurs during deep sleep as well as local sleep in awake individuals and is thought to suppress sensory processing and promote synaptic plasticity (Quercia et al., 2018). To investigate whether synchronization between R5 and helicon play a role in suppressing visual processing to regulate locomotion during sleep, we used optogenetics to separately and simultaneously activate these networks at 1 Hz in sleeping flies **(Fig. 5E)**. After sleep deprivation, sleeping flies were exposed to green light to arouse them and elicit visually evoked locomotion while simultaneously applying red light pulses at 1 Hz for optogenetic stimulation **(Fig. 5E)**. As shown for rested control flies **(compare Fig. 3I)**, all genotypes showed slight arousal at the beginning of the red light stimulation **(Fig. 5F and S4A, B).** However, as expected, helicon cell stimulation led to the strongest degree of arousal **(Fig. S4A)** with most flies being awakened **(Fig. S4B),** while arousal during R5 stimulation was consistent with the control **(Fig. S4A)**. During green light stimulation, control flies and helicon activation showed the highest degree of visually induced locomotion **(Fig. 5G-H)**. In contrast, visually triggered locomotion was not observed during stimulation of R5 neurons. As shown before, flies are capable of reacting to sensory stimuli during R5 stimulation **(Fig. 3J)**. Interestingly, compared to R5 activation alone, synchronous activation of R5 and helicon led to a stronger reduction of locomotor activity **(Fig. 5G)** and only a small fraction of flies were awakened by green light **(Fig. S4B)**, indicating that R5 and helicon synchronization further facilitates the suppression of behavioral responsiveness to visual stimuli. This indicates that sleep drive mediated by R5 neurons overrides gating of locomotion by helicon cells and further demonstrates that synchronization between these networks locks the locomotion-initiating networks into a state that, dependent on sleep need, reduces sensory processing and behavioral responsiveness.

R5 oscillations modulate neural activity in head direction neurons

In principle, the predominantly GABAergic ring neurons (Hanesch et al., 1989) could suppress locomotion by directly interacting with helicon cells. However, our optogenetic experiments revealed no direct influence of R5 neurons on helicon cell membrane potential or intracellular Ca^{2+} (data not shown). We therefore again turned to the connectome and found that helicon cells as well as R5 neurons are connected to EPG neurons **(Fig. 6A)**, which are functionally analogous to mammalian head-direction

neurons, representing the fly's heading direction and initiating body turns towards or away from sensory stimuli (Green et al., 2017; Turner-Evans et al., 2017; Vafidis et al., 2021). As most synaptic connections to helicon and R5 are found within the ring **(Fig. 6A)**, we focused on this structure and used ArcLight to test whether EPG compound electrical activity is subject to circadian modulation **(Fig. 6B, C)**. In the morning, EPG neurons display non-oscillatory spontaneous events that were mostly comprised by a hyperpolarization followed by a rebound depolarization **(Fig. 6C).** Depolarizations occurred at an average rate of 1.2 every 10s and generated a peak in the power spectrum between 0.1 and 0.2 Hz, which was markedly reduced at night compared to the morning **(Fig. 6D).** We next tested whether R5 could be responsible for reducing spontaneous activity in the EPG network at night **(Fig. 6E-H)**. In fact, we found that activating R5 hyperpolarizes EPG neurons **(Fig. 6F)**. Moreover, imposing a 1 Hz activity pattern on R5 neurons induced transient 1 Hz hyperpolarization in EPG neurons **(Fig. 6G)** and completely abolished spontaneous events usually observed during the morning hours **(Fig. 6H)**. As such strong hyperpolarizations are not present in the EPG network during natural conditions, the excitatory locomotion gating input from helicon and the inhibitory input from R5 might cancel each other out when helicon and R5 synchronize at night. In fact, we found that for about 80% of R5-EPG synapses the nearest non-R5 Euclidian neighbor were helicon-EPG synapses **(Fig. 6I-K)**. Interestingly, within the inner parts of the ring, where there are no R5 synapses, helicon-EPG synapses can be found in close proximity to synaptic input of sleep-regulating R3 neurons (Aleman et al., 2021; Hulse et al., 2021) **(Fig. 6J)**, indicating that these synaptic motifs and their spatial relations are indeed major sites of integrating navigation and sleep regulation. Taken together, we propose that inhibition of EPG activity mediated through R5 might be a crucial component for fine-tuning navigation during the day as well as modulating behavioral responsiveness and sleep depth during the night.

Discussion

Coherent SWA across the cortex is a hallmark of human deep sleep (Adamantidis et al., 2019; Buzsaki and Draguhn, 2004), but how these oscillations control arousal thresholds to promote sleep maintenance remains unclear to this day. Here, we demonstrate how

sleep need in *Drosophila* generates coherent oscillations between different neural networks to reduce the functional connectivity between locomotion gating networks and the navigational system. We therefore provide mechanistic insight into how network interactions generate SWA to establish a sensory gate by impeding behavioral responses to external stimuli.

Generating SWA is inherent to neural networks

In this work we discovered that sleep need elicits oscillatory signatures within a previously described recurrent circuitry (Donlea et al., 2018). At night, the master sleep homeostat, the dFSB, increases excitability (Kempf et al., 2019) to generate compound oscillations without single-unit synchronization (**Fig. 1**), suggesting that the dFSB oscillates cell-autonomously. In contrast, compound oscillations in R5 are promoted by single-unit synchronizations and can be driven by TuBu neurons which receive circadian input (Guo et al., 2018; Lamaze et al., 2018; Raccuglia et al., 2019). Interestingly, we discovered that dependent on the circadian clock the dFSB and the R5 network reciprocally facilitate presynaptic Ca^{2+} oscillations (**Fig. 2**), most likely through the interconnecting helicon cells, which can also display oscillatory signatures (**Fig. 4, 5**). While it was previously described that the dFSB hyperpolarizes helicon at the single cell level (Donlea et al., 2018), we here show at the network level, in addition to this hyperpolarization, that the dFSB increases helicon presynaptic Ca^{2+} levels and elicits oscillations (**Fig. 4**). These observations could be explained by hyperpolarization-activated Ca^{2+}-permeable channels similar to Ih channels. Interestingly, Ih channels are at the basis of cell-autonomous thalamic oscillations which are crucial for promoting sleep in mammals (Kanyshkova et al., 2009; McCormick and Pape, 1990). We previously found that TuBu neurons (Raccuglia et al., 2019) upstream of R5, and now the head direction neurons (EPG) downstream of R5 and helicon did not show spontaneous SWA (**Fig. 6**), indicating that oscillations might be restricted to the recurrent sleep circuitry. Similar to neural oscillations in mammalian circuits, we observed slight changes in the power spectrum of spontaneous SWA compared to the SWA induced by activating specific circuits. This is likely explained by the fact that the precise power and frequency of SWA depends on a complex interplay between different neural circuits (Neske, 2015).

In mammalian brains, *in vivo* and *in vitro* recordings have shown that even relatively small isolated cortical and thalamic circuits have the ability to generate SWA (Neske, 2015), indicating that some networks oscillate autonomously. 'Local sleep' provides further evidence for this, describing the network-specific occurrence of a sleep-like state in awake individuals in which the locus of the oscillations depends on the previously performed tasks (Hung et al., 2013; Quercia et al., 2018). Moreover, cortical networks that are heavily engaged in a task when awake exhibit comparably stronger SWA during subsequent deep sleep (Huber et al., 2004), demonstrating that sensory processing and homeostatic sleep regulation are intertwined. These findings accumulate to the current understanding that sleep need is experienced by specific networks and that the generation of SWA is a means to suppress sensory processing and promote synaptic plasticity. Our findings in *Drosophila* further substantiate the notion that SWA is inherent to sleep-regulating neural circuits and that network coherence might be an evolutionarily optimized strategy to suppress sensory processing in order to induce and maintain quiescent states (Suárez-Grimalt and Raccuglia, 2021).

Coherent network oscillations establish a sensory gate for the maintenance of quiescent states

We here describe neural interactions within a sleep-circuitry that has intriguing functional and physiological analogies to thalamocortical interactions in mammalian brains. The thalamus functions as a relay station for sensory signals and motor commands, essentially regulating behavioral responsiveness to external stimuli (Andrillon and Kouider, 2020). Cortical synchronizations are orchestrated by thalamocortical interactions (Gent et al., 2018) and are mechanistically at the basis of elevated arousal thresholds during deep sleep. However, how exactly coherent oscillations can act as a gate during sleep remains unclear.

Here, our work provides mechanistic insight demonstrating how, akin to thalamocortical oscillations, the dFSB (**Fig. 1**) act as a switch to synchronize electrical patterns between arousal mediating helicon and sleep need mediating R5 which reduced behavioral responsiveness to external stimuli (**Fig. 5**). Reduced responsiveness is most likely achieved by the fact that both helicon and R5 target the head direction system (**Fig. 6**), which is part of a navigational system that allows flies to orientate themselves in their

surroundings (Seelig and Jayaraman, 2013; Turner-Evans et al., 2017). During synchronized oscillations the functionally antagonistic inputs of helicon and R5 to the head direction system cancel each other out to maintain a quiescent state. This would infer that arousability inversely correlates with the degree of synchrony between networks, which is substantiated by our finding that compared to R5 activation alone, synchronized activation of helicon and R5 further facilitates the suppression of behavioral responsiveness (**Fig. 5 and S4**). We propose that this is a mechanistic basis for reduced arousability that correlate to a quiescent state that is less influenced by external cues, facilitating the shift from an allocentric-like to an egocentric-like worldview.

With increasing sleep need GABAergic R5 neurons increase their presynaptic weight (Liu et al., 2016), which tilts the head direction system to more inhibition. While similar interactions have recently been proposed as part of a theoretical model (Flores-Valle et al., 2021), we here provide experimental evidence for this, demonstrating that rhythmic R5 activity hyperpolarizes the head direction system to suppress spontaneous events (**Fig. 6**). The degree of synchronizations as well as the balance between excitation and inhibition can thus determine the arousal threshold during quiescent states.

Sleep, navigation and postural control

One of the main functions of SWA during sleep has been shown to be the promotion of synaptic plasticity to consolidate experiences made during the day, providing the foundation for long-term memories (Klinzing et al., 2019). The circuitry we investigated in this work unifies visual processing, locomotion, navigation and sleep regulation. Ring neurons in general have been shown to play a role in visual place learning (Ofstad et al., 2011) and it is likely, that the oscillatory coherence reported here facilitates synaptic plasticity to update the navigational system. Theoretical work has proposed that R5 could balance Hebbian plasticity in the navigational system by alternating between oscillatory and non-oscillatory states and by modulating the synaptic weights to head direction neurons (Flores-Valle et al., 2021). Besides their role in navigation, we found that frequency-specific activation of R5 to mimic SWA induced a quiescent state accompanied by grooming (**Fig. 3**). Grooming behavior in *Drosophila* is regulated by the circadian clock (Qiao et al., 2018) and occurs predominantly during short resting phases

prior to night time sleep. Therefore, grooming could be considered a preparatory stage for sleep (Qiao et al., 2018) and the activation of R5 might promote this preparatory stage eventually leading to sleep. Moreover, we observed that activating R5 at 10 Hz leads to flies losing postural control and behavioral responsiveness entirely (**Fig. 3**), indicating that coherent oscillations in *Drosophila* might also provide the neurophysiological basis for maintaining postural control during quiescent states. The fine balance of R5 network activity therefore appears to not only mediate sleep regulation but also provide a system for maintaining the basis for further locomotion-based behavioral programs, such as upright posture.

As R5 neurons receive synaptic inputs from visual neurons, it is conceivable that these inhibitory neurons initially played a role in navigation alone and later evolved to suppress locomotor activity to facilitate quiescent states, which promote synaptic plasticity by means of interconnecting networks through synchronized SWA. As excitatory (helicon) and inhibitory (R5) inputs likely cancel each other out at the level of the EPG network, synchronizations reduce the functional connectivity between systems that promote the initiation of behavioral programs. This is in accordance with previous findings showing that activation of the dFSB leads to neural networks being unresponsive to sensory stimuli, thus reducing behavioral responsiveness (Tainton-Heap et al., 2021). Salient sensory stimuli might be able to break up synchronized states by engaging additional neurons or specific engrams, thus acutely increasing functional connectivity, which might lead to flies waking up and reacting to external stimuli (French et al., 2021). The neural interactions we discovered and discussed in this work are not restricted to flies, but most likely represent the mechanistic basis for regulating waking and sleep across phyla (Tononi and Massimini, 2008).

Acknowledgements

We thank the Janelia fly project and the Bloomington Stock Center.

Funding

This project was funded by the Deutsche Forschungsgemeinschaft (DFG, German Research Foundation) under Germany´s Excellence Strategy – EXC-2049 – 390688087, the Emmy Noether Programme, TP A27 of SFB958 (184695641) and TP A07 of SFB1315 (327654276) to D.O. D.O. was further supported by FOR 2705 (365082554). D.R. was supported by the DFG grant 462539941. R.S-G. was supported by a PhD fellowship from the Einstein Center for Neurosciences Berlin.

Author contribution

Conceptualization: D.R., R.S-G. and D.O.

Investigation: D.R., R.S-G. and C.B.

Resources: D.R., J.R.G. and D.O.

Writing: D.R., R.S-G. and D.O.

Authors declare no competing interests.

References

Adamantidis, A.R., Gutierrez Herrera, C., and Gent, T.C. (2019). Oscillating circuitries in the sleeping brain. Nat Rev Neurosci *20*, 746-762.

Aleman, A., Omoto, J.J., Singh, P., Nguyen, B.-C., Kandimalla, P., Hartenstein, V., and Donlea, J.M. (2021). Opposing subclasses of Drosophila ellipsoid body neurons promote and suppress sleep. bioRxiv, 2021.2010.2019.464469.

Andrillon, T., and Kouider, S. (2020). The vigilant sleeper: neural mechanisms of sensory (de)coupling during sleep. Current Opinion in Physiology *15*, 47-59.

Buzsaki, G., and Draguhn, A. (2004). Neuronal oscillations in cortical networks. Science *304*, 1926-1929.

Cao, G., Platisa, J., Pieribone, V.A., Raccuglia, D., Kunst, M., and Nitabach, M.N. (2013). Genetically targeted optical electrophysiology in intact neural circuits. Cell *154*, 904-913.

Claridge-Chang, A., Roorda, R.D., Vrontou, E., Sjulson, L., Li, H., Hirsh, J., and Miesenbock, G. (2009). Writing memories with light-addressable reinforcement circuitry. Cell *139*, 405-415.

Crunelli, V., and Hughes, S.W. (2010). The slow (<1 Hz) rhythm of non-REM sleep: a dialogue between three cardinal oscillators. Nat Neurosci *13*, 9-17.

Donlea, J.M. (2019). Roles for sleep in memory: insights from the fly. Curr Opin Neurobiol *54*, 120-126.

Donlea, J.M., Pimentel, D., and Miesenbock, G. (2014). Neuronal machinery of sleep homeostasis in Drosophila. Neuron *81*, 860-872.

Donlea, J.M., Pimentel, D., Talbot, C.B., Kempf, A., Omoto, J.J., Hartenstein, V., and Miesenbock, G. (2018). Recurrent Circuitry for Balancing Sleep Need and Sleep. Neuron *97*, 378-389 e374.

Donlea, J.M., Ramanan, N., and Shaw, P.J. (2009). Use-dependent plasticity in clock neurons regulates sleep need in Drosophila. Science *324*, 105-108.

Flores-Valle, A., Goncalves, P.J., and Seelig, J.D. (2021). Integration of sleep homeostasis and navigation in Drosophila. PLoS Comput Biol *17*, e1009088.

French, A.S., Geissmann, Q., Beckwith, E.J., and Gilestro, G.F. (2021). Sensory processing during sleep in Drosophila melanogaster. Nature *598*, 479-482.

Gent, T.C., Bandarabadi, M., Herrera, C.G., and Adamantidis, A.R. (2018). Thalamic dual control of sleep and wakefulness. Nat Neurosci *21*, 974-984.

Green, J., Adachi, A., Shah, K.K., Hirokawa, J.D., Magani, P.S., and Maimon, G. (2017). A neural circuit architecture for angular integration in Drosophila. Nature *546*, 101-106.

Guo, F., Holla, M., Diaz, M.M., and Rosbash, M. (2018). A Circadian Output Circuit Controls Sleep-Wake Arousal in Drosophila. Neuron *100*, 624-635 e624.

Hanesch, U., Fischbach, K.F., and Heisenberg, M. (1989). Neuronal architecture of the central complex in Drosophila melanogaster. Cell and Tissue Research *257*, 343-366.

Huber, R., Ghilardi, M.F., Massimini, M., and Tononi, G. (2004). Local sleep and learning. Nature *430*, 78-81.

Hulse, B.K., Haberkern, H., Franconville, R., Turner-Evans, D.B., Takemura, S., Wolff, T., Noorman, M., Dreher, M., Dan, C., Parekh, R*., et al.* (2021). A connectome of the Drosophila central complex reveals network motifs suitable for flexible navigation and context-dependent action selection. Elife 10.

Hung, C.S., Sarasso, S., Ferrarelli, F., Riedner, B., Ghilardi, M.F., Cirelli, C., and Tononi, G. (2013). Local experience-dependent changes in the wake EEG after prolonged wakefulness. Sleep *36*, 59-72.

Kannan, M., Vasan, G., Huang, C., Haziza, S., Li, J.Z., Inan, H., Schnitzer, M.J., and Pieribone, V.A. (2018). Fast, in vivo voltage imaging using a red fluorescent indicator. Nat Methods *15*, 1108-1116.

Kanyshkova, T., Pawlowski, M., Meuth, P., Dube, C., Bender, R.A., Brewster, A.L., Baumann, A., Baram, T.Z., Pape, H.C., and Budde, T. (2009). Postnatal expression pattern of HCN channel isoforms in thalamic neurons: relationship to maturation of thalamocortical oscillations. J Neurosci *29*, 8847-8857.

Kempf, A., Song, S.M., Talbot, C.B., and Miesenbock, G. (2019). A potassium channel beta-subunit couples mitochondrial electron transport to sleep. Nature *568*, 230-234.

Klapoetke, N.C., Murata, Y., Kim, S.S., Pulver, S.R., Birdsey-Benson, A., Cho, Y.K., Morimoto, T.K., Chuong, A.S., Carpenter, E.J., Tian, Z*., et al.* (2014). Independent optical excitation of distinct neural populations. Nat Methods *11*, 338-346.

Klinzing, J.G., Niethard, N., and Born, J. (2019). Mechanisms of systems memory consolidation during sleep. Nat Neurosci *22*, 1598-1610.

Krueger, J.M., Nguyen, J.T., Dykstra-Aiello, C.J., and Taishi, P. (2019). Local sleep. Sleep Med Rev *43*, 14-21.

Lamaze, A., Kratschmer, P., Chen, K.F., Lowe, S., and Jepson, J.E.C. (2018). A Wake-Promoting Circadian Output Circuit in Drosophila. Curr Biol *28*, 3098-3105 e3093.

Leung, L.C., Wang, G.X., Madelaine, R., Skariah, G., Kawakami, K., Deisseroth, K., Urban, A.E., and Mourrain, P. (2019). Neural signatures of sleep in zebrafish. Nature *571*, 198-204.

Liu, S., Liu, Q., Tabuchi, M., and Wu, M.N. (2016). Sleep Drive Is Encoded by Neural Plastic Changes in a Dedicated Circuit. Cell *165*, 1347-1360.

Low, P.S., Shank, S.S., Sejnowski, T.J., and Margoliash, D. (2008). Mammalian-like features of sleep structure in zebra finches. Proc Natl Acad Sci U S A *105*, 9081-9086.

McCormick, D.A., and Pape, H.C. (1990). Properties of a hyperpolarization-activated cation current and its role in rhythmic oscillation in thalamic relay neurones. J Physiol *431*, 291-318.

Mohammad, F., Stewart, J.C., Ott, S., Chlebikova, K., Chua, J.Y., Koh, T.W., Ho, J., and Claridge-Chang, A. (2017). Optogenetic inhibition of behavior with anion channelrhodopsins. Nat Methods *14*, 271-274.

Neske, G.T. (2015). The Slow Oscillation in Cortical and Thalamic Networks: Mechanisms and Functions. Front Neural Circuits *9*, 88.

Ofstad, T.A., Zuker, C.S., and Reiser, M.B. (2011). Visual place learning in Drosophila melanogaster. Nature *474*, 204-207.

Pimentel, D., Donlea, J.M., Talbot, C.B., Song, S.M., Thurston, A.J.F., and Miesenbock, G. (2016). Operation of a homeostatic sleep switch. Nature *536*, 333-337.

Qiao, B., Li, C., Allen, V.W., Shirasu-Hiza, M., and Syed, S. (2018). Automated analysis of long-term grooming behavior in Drosophila using a k-nearest neighbors classifier. Elife *7*.

Quercia, A., Zappasodi, F., Committeri, G., and Ferrara, M. (2018). Local Use-Dependent Sleep in Wakefulness Links Performance Errors to Learning. Front Hum Neurosci *12*, 122.

Raccuglia, D., Huang, S., Ender, A., Heim, M.M., Laber, D., Suarez-Grimalt, R., Liotta, A., Sigrist, S.J., Geiger, J.R.P., and Owald, D. (2019). Network-Specific Synchronization of Electrical Slow-Wave Oscillations Regulates Sleep Drive in Drosophila. Curr Biol *29*, 3611-3621 e3613.

Raccuglia, D., McCurdy, L.Y., Demir, M., Gorur-Shandilya, S., Kunst, M., Emonet, T., and Nitabach, M.N. (2016). Presynaptic GABA Receptors Mediate Temporal Contrast Enhancement in Drosophila Olfactory Sensory Neurons and Modulate Odor-Driven Behavioral Kinetics. eNeuro *3*.

Ramon, F., Hernandez-Falcon, J., Nguyen, B., and Bullock, T.H. (2004). Slow wave sleep in crayfish. Proc Natl Acad Sci U S A *101*, 11857-11861.

Sanchez-Vives, M.V., and McCormick, D.A. (2000). Cellular and network mechanisms of rhythmic recurrent activity in neocortex. Nat Neurosci *3*, 1027-1034.

Scheffer, L.K., Xu, C.S., Januszewski, M., Lu, Z., Takemura, S.Y., Hayworth, K.J., Huang, G.B., Shinomiya, K., Maitlin-Shepard, J., Berg, S.*, et al.* (2020). A connectome and analysis of the adult Drosophila central brain. Elife *9*.

Seelig, J.D., and Jayaraman, V. (2013). Feature detection and orientation tuning in the Drosophila central complex. Nature *503*, 262-266.

Shaw, P.J., Cirelli, C., Greenspan, R.J., and Tononi, G. (2000). Correlates of sleep and waking in Drosophila melanogaster. Science *287*, 1834-1837.

Shein-Idelson, M., Ondracek, J.M., Liaw, H.P., Reiter, S., and Laurent, G. (2016). Slow waves, sharp waves, ripples, and REM in sleeping dragons. Science *352*, 590-595.

Siclari, F., and Tononi, G. (2017). Local aspects of sleep and wakefulness. Curr Opin Neurobiol *44*, 222-227.

Sitaraman, D., Aso, Y., Rubin, G.M., and Nitabach, M.N. (2015). Control of Sleep by Dopaminergic Inputs to the Drosophila Mushroom Body. Front Neural Circuits *9*, 73.

Suárez-Grimalt, R., and Raccuglia, D. (2021). The neural architecture of sleep regulation – insights from Drosophila. Neuroforum *27*, 189-199.

Tainton-Heap, L.A.L., Kirszenblat, L.C., Notaras, E.T., Grabowska, M.J., Jeans, R., Feng, K., Shaw, P.J., and van Swinderen, B. (2021). A Paradoxical Kind of Sleep in Drosophila melanogaster. Curr Biol *31*, 578-590 e576.

Tononi, G., and Massimini, M. (2008). Why does consciousness fade in early sleep? Ann N Y Acad Sci *1129*, 330-334.

Troup, M., Yap, M.H., Rohrscheib, C., Grabowska, M.J., Ertekin, D., Randeniya, R., Kottler, B., Larkin, A., Munro, K., Shaw, P.J.*, et al.* (2018). Acute control of the sleep switch in Drosophila reveals a role for gap junctions in regulating behavioral responsiveness. Elife *7*.

Turner-Evans, D., Wegener, S., Rouault, H., Franconville, R., Wolff, T., Seelig, J.D., Druckmann, S., and Jayaraman, V. (2017). Angular velocity integration in a fly heading circuit. Elife *6*.

Vafidis, P., Owald, D., D'Albis, T., and Kempter, R. (2021). Learning accurate path integration in a ring attractor model of the head direction system. bioRxiv, 2021.2003.2012.435035.

Vyazovskiy, V.V., Olcese, U., Hanlon, E.C., Nir, Y., Cirelli, C., and Tononi, G. (2011). Local sleep in awake rats. Nature *472*, 443-447.

Yap, M.H.W., Grabowska, M.J., Rohrscheib, C., Jeans, R., Troup, M., Paulk, A.C., van Alphen, B., Shaw, P.J., and van Swinderen, B. (2017). Oscillatory brain activity in spontaneous and induced sleep stages in flies. Nat Commun *8*, 1815.

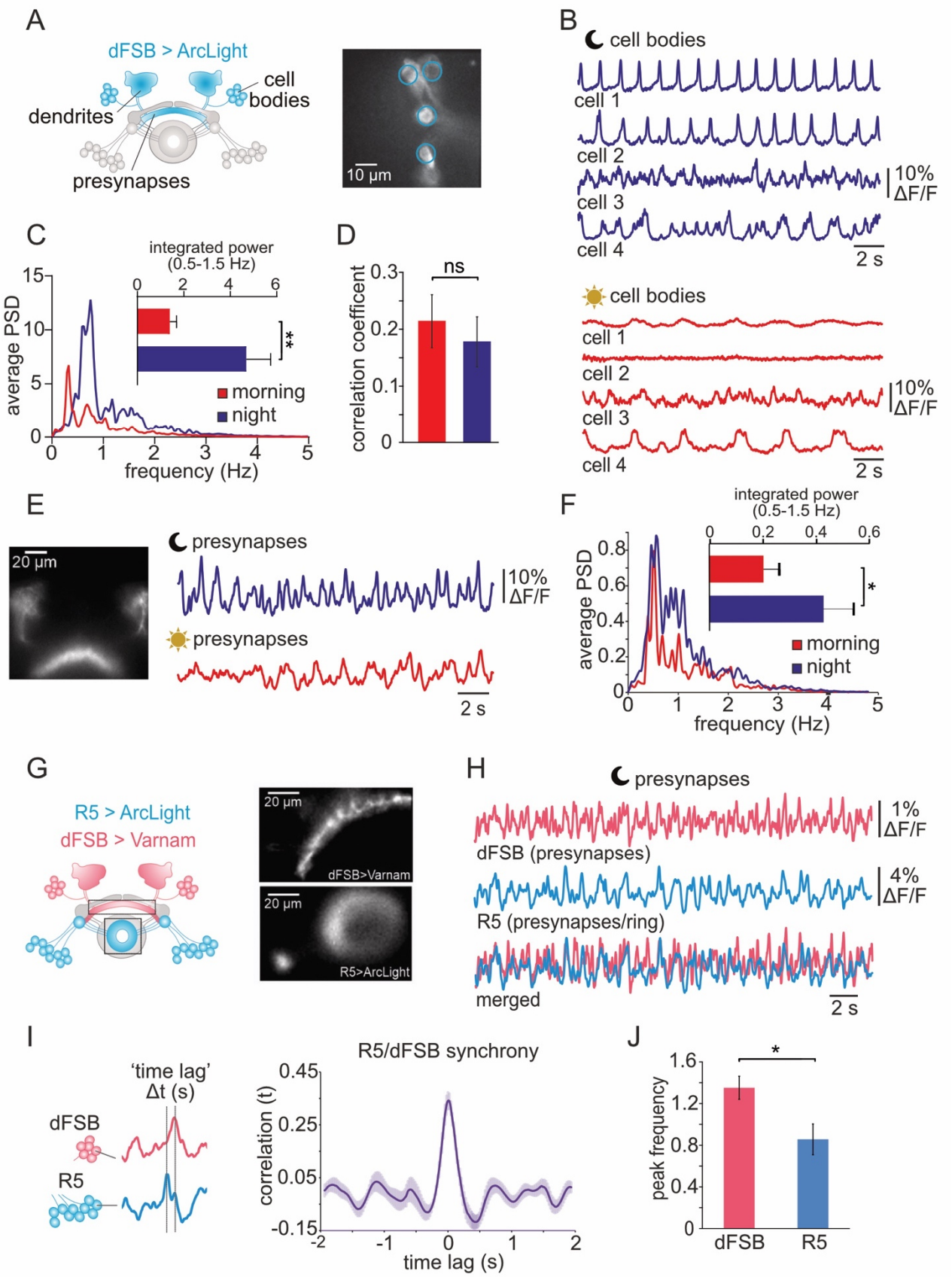
A
dFSB > ArcLight
cell bodies
dendrites
presynapses
10 µm
B
cell bodies
cell 1
cell 2
cell 3
cell 4
10% ΔF/F
2 s
cell bodies
cell 1
cell 2
cell 3
cell 4
10% ΔF/F
2 s
C
integrated power (0.5-1.5 Hz)
average PSD
frequency (Hz)
morning
night
**
D
ns
correlation coefficent
E
20 µm
presynapses
10% ΔF/F
presynapses
2 s
F
integrated power (0.5-1.5 Hz)
average PSD
frequency (Hz)
morning
night
*
G
R5 > ArcLight
dFSB > Varnam
20 µm
dFSB>Varnam
20 µm
R5>ArcLight
H
presynapses
1% ΔF/F
dFSB (presynapses)
4% ΔF/F
R5 (presynapses/ring)
merged
2 s
I
'time lag' Δt (s)
dFSB
R5
R5/dFSB synchrony
correlation (t)
time lag (s)
J
*
peak frequency
dFSB
R5

Figure 1. Neural circuits mediating sleep drive display slow-wave coherence.
(A) Left: schematic of a sleep regulating circuitry composed of dorsal fan-shaped body (dFSB, highlighted), helicon cells and R5 neurons. Recording sites are indicated for single-unit and compound recordings. Right: wide-field image of cell bodies expressing the voltage indicator ArcLight under the control of 23E10-GAL4. **(B)** *Ex vivo* multi-cellular voltage imaging of individual dFSB neurons recorded in the morning (ZT 2-4) and at night (ZT 14-15). **(C)** Average power spectrum of single-cell voltage recordings showing increased slow-wave power (0.5-1.5 Hz) at night (n=23 for ZT 2-4 and n= 34 for ZT 14-15, Mann-Whitney test). **(D)** Correlation between electrical patterns of individual cell bodies is similar in the morning and at night (n=30-39, Mann-Whitney test). **(E)** Wide-field image of dFSB neurites and compound recordings of presynaptic electrical activity recorded in the morning (ZT 2-4) and at night (ZT 14-15). **(F)** Average power spectra of compound oscillations in dFSB presynapses. Compound integrated slow-wave power (0.5-1.5 Hz) is increased at night (n=9-10, Mann-Whitney test). **(G)** Wide-field image and schematic of dFSB neurons expressing Varnam (23E10-LexA) and R5 neurons simultaneously expressing ArcLight (88F06-GAL4). Rectangles indicate recording sites. **(H)** Example recording of R5 and dFSB electrical patterns recorded at night (ZT 14-15). **(I)** Cross correlogram of electrical patterns of R5 and dFSB (n=10) indicates a large overlap of slow-wave activity. **(J)** Peak frequency distribution indicating increased oscillatory frequencies in dFSB presynapses (n=9-10, Mann-Whitney test). In all panels, significance is represented as follows: *$p \leq 0.05$ and **$p \leq 0.01$.

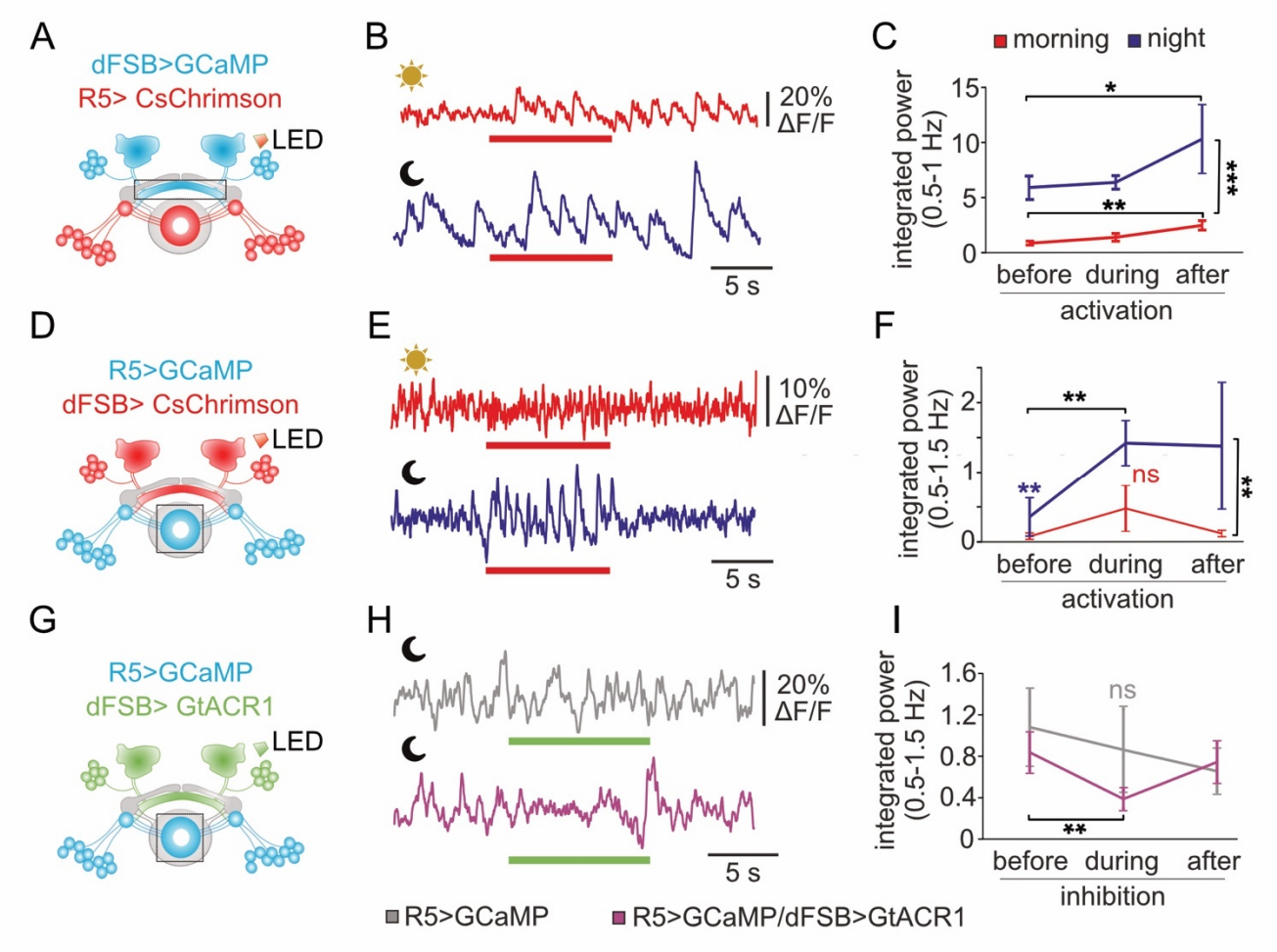
A
dFSB>GCaMP
R5> CsChrimson
LED
B
20%
ΔF/F
5 s
C
morning
night
integrated power
(0.5-1 Hz)
15
10
5
0
*
**
***
before
during
after
activation
D
R5>GCaMP
dFSB> CsChrimson
LED
E
10%
ΔF/F
5 s
F
integrated power
(0.5-1.5 Hz)
2
1
0
**
ns
**
**
before
during
after
activation
G
R5>GCaMP
dFSB> GtACR1
LED
H
20%
ΔF/F
5 s
I
integrated power
(0.5-1.5 Hz)
1.6
1.2
0.8
0.4
0
ns
**
before
during
after
inhibition
R5>GCaMP
R5>GCaMP/dFSB>GtACR1

Figure 2: Reciprocal facilitation of SWA between sleep drive mediating circuits is modulated by the circadian clock.

(A, D, G) Schematic overview of presynaptic recording sites and sites of optogenetic activation and inhibition. **(B)** Example traces of dFSB presynaptic Ca^{2+} activity (23E10-GAL4) during optogenetic activation of R5 neurons (58H05-LexA) in the morning (ZT 2-6) and at night (ZT 14-18). **(C)** Slow-wave power (0.5-1 Hz) in the dFSB increases after optogenetic stimulation of R5 neurons (*n*=10, Friedman test with post hoc Dunn's multiple comparisons test). Pooling the data for during and after stimulation indicates that inducing oscillations is facilitated at night (*n*=20, Mann-Whitney test). **(E)** Example traces of R5 presynaptic Ca^{2+} activity (58H05-GAL4) during optogenetic activation of dFSB neurons (23E10-LexA) in the morning (ZT 2-6) and at night (ZT 14-18). **(F)** At night but not in the morning R5 slow-wave power (0.5-1.5 Hz) increases during optogenetic stimulation of R5 neurons (*n*=10-11, Friedman test with post hoc Dunn's multiple comparisons test). Pooling the data for during and after stimulation indicates that inducing oscillations is facilitated at night (*n*=20-22, Mann-Whitney test). **(H)** Example traces of R5 presynaptic Ca^{2+} activity (58H05-LexA) during optogenetic inhibition of dFSB neurons (23E10-GAL4) in the morning. **(I)** Slow-wave power (0.5-1.5 Hz) is reduced when hyperpolarizing dFSB neurons (*n*=6-7, Friedman test with post hoc Dunn's multiple comparisons test). In all panels, significance is represented as follows: *$p \leq 0.05$ and **$p \leq 0.01$.

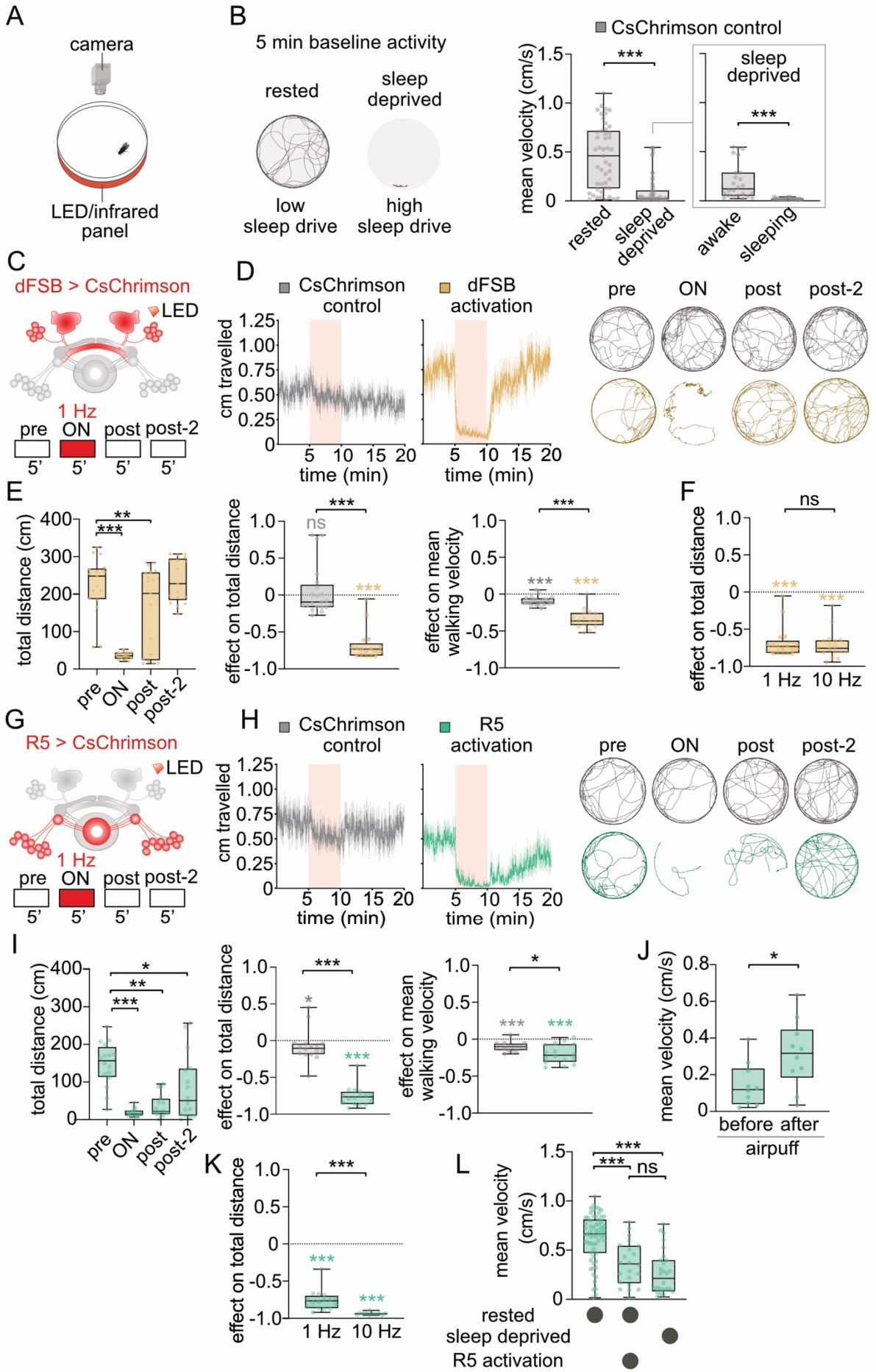
A
camera
LED/infrared panel
B
5 min baseline activity
rested
sleep deprived
low sleep drive
high sleep drive
CsChrimson control
mean velocity (cm/s)
sleep deprived
rested
sleep deprived
awake
sleeping
C
dFSB > CsChrimson
LED
1 Hz
pre ON post post-2
5' 5' 5' 5'
D
CsChrimson control
dFSB activation
cm travelled
time (min)
pre ON post post-2
E
total distance (cm)
pre ON post post-2
effect on total distance
effect on mean walking velocity
F
effect on total distance
1 Hz 10 Hz
G
R5 > CsChrimson
LED
1 Hz
pre ON post post-2
5' 5' 5' 5'
H
CsChrimson control
R5 activation
cm travelled
time (min)
pre ON post post-2
I
total distance (cm)
pre ON post post-2
effect on total distance
effect on mean walking velocity
J
mean velocity (cm/s)
before after
airpuff
K
effect on total distance
1 Hz 10 Hz
L
mean velocity (cm/s)
rested
sleep deprived
R5 activation

Figure 3. Neural circuits mediating sleep drive acutely control locomotor behavior.
(A) The effect of activation on locomotion is evaluated by tracking the fly's position in a circular arena. **(B)** Locomotion of individual flies provides information about the animal's internal state. Left: example trajectories over a 5 min baseline of a rested and a sleep deprived +>LexAop-CsChrimson control fly. Right: baseline velocity of sleep-deprived flies during a 5 min period is reduced compared to that of rested flies (*n*=43 for rested and *n*=55 for sleep deprived, Mann-Whitney test). Sleep deprived flies can either meet the sleep criteria (5 min of inactivity, 'sleeping', *n*=31) or be active ('awake', *n*=24). **(C)** Schematic overview of the optogenetic protocol used to activate dFSB under 23E10-GAL4 control. After 5 min of baseline activity ('pre'), flies were exposed to 5 min of 5 ms red light pulses at 1 Hz ('ON') and allowed to recover for 10 min ('post' and 'post-2'). **(D)** Left: average locomotion traces, *n*=19 for CsChrimson control (+ retinal) and *n*=17 for dFSB activation (+ retinal). Curves: mean ± SEM. Right: example trajectories of genotypes tested. **(E)** 1 Hz dFSB activation decreases locomotion of rested flies during and after activation (panel 1, *n*=17, Friedman test with Dunn's multiple comparisons). Optogenetic stimulation reduced total distance travelled and mean velocity of walking flies (panel 2 and 3) of 23E10-GAL4>UAS-CsChrimson flies compared to control flies, *n*=17-19, Mann-Whitney test (comparisons between genotypes, black asterisks) and Wilcoxon signed-rank test (comparisons to baseline locomotion, colorful asterisks). The effect of the stimulation is calculated by normalizing locomotion parameters to baseline (ie. (total distance [during] – total distance [baseline]) / (total distance [during] + total distance [baseline])). **(F)** The effect of 1 Hz dFSB stimulation on distance travelled did not differ between different frequencies of activation (*n*= 17 each, Mann-Whitney test). **(G)** The same optogenetic protocol described in **C** is used to activate R5 neurons under 58H05-GAL4 control. **(H)** Left: average locomotion traces, *n*=16 for CsChrimson control (+ retinal) and *n*=16 for R5 activation (+ retinal). Curves: mean ± SEM. Right: example trajectories of genotypes tested. **(I)** 1 Hz stimulation reduced distance travelled during and after activation (panel 1), *n*=16, Friedman test with Dunn's multiple comparisons. Optogenetic activation decreased distance travelled and mean velocity of walking 58H05-GAL4>UAS-CsChrimson flies compared to control flies (panel 2 and 3), *n*=16, Mann-Whitney test (comparisons between genotypes, black asterisks) and Wilcoxon signed-rank test (comparisons to baseline locomotion, colored asterisks). **(J)** Exposure to a 10s-long air puff during R5 activation at 1 Hz increased the mean velocity of rested 58H05-GAL4>UAS-CsChrimson flies (+ retinal, *n*=10, Wilcoxon matched-pairs signed rank test). **(K)** The effect of 1 Hz R5 stimulation on distance travelled differed between different frequencies of activation (*n*=16 for 1 Hz and *n*=11 for 10 Hz, Mann-Whitney test). **(L)** Mean walking velocity of 58H05-LexA>LexAop-CsChrimson of rested flies (+ retinal) was reduced when R5 was activated at 1 H, resembling the locomotion levels of awake sleep-deprived flies (+ retinal), *n*=63 for rested, *n*=22 for rested+R5 activation, *n*=28 for sleep deprived, Kruskal-Wallis test with Dunn's multiple comparisons). Experiments shown in this figure were done during the subjective day of the flies (ZT 1-10). In all panels, box-plots show median (line), quartiles (boxes) and range (whiskers) and significance is represented as follows: *$p \leq 0.05$, **$p \leq 0.01$ and ***$p \leq 0.001$.

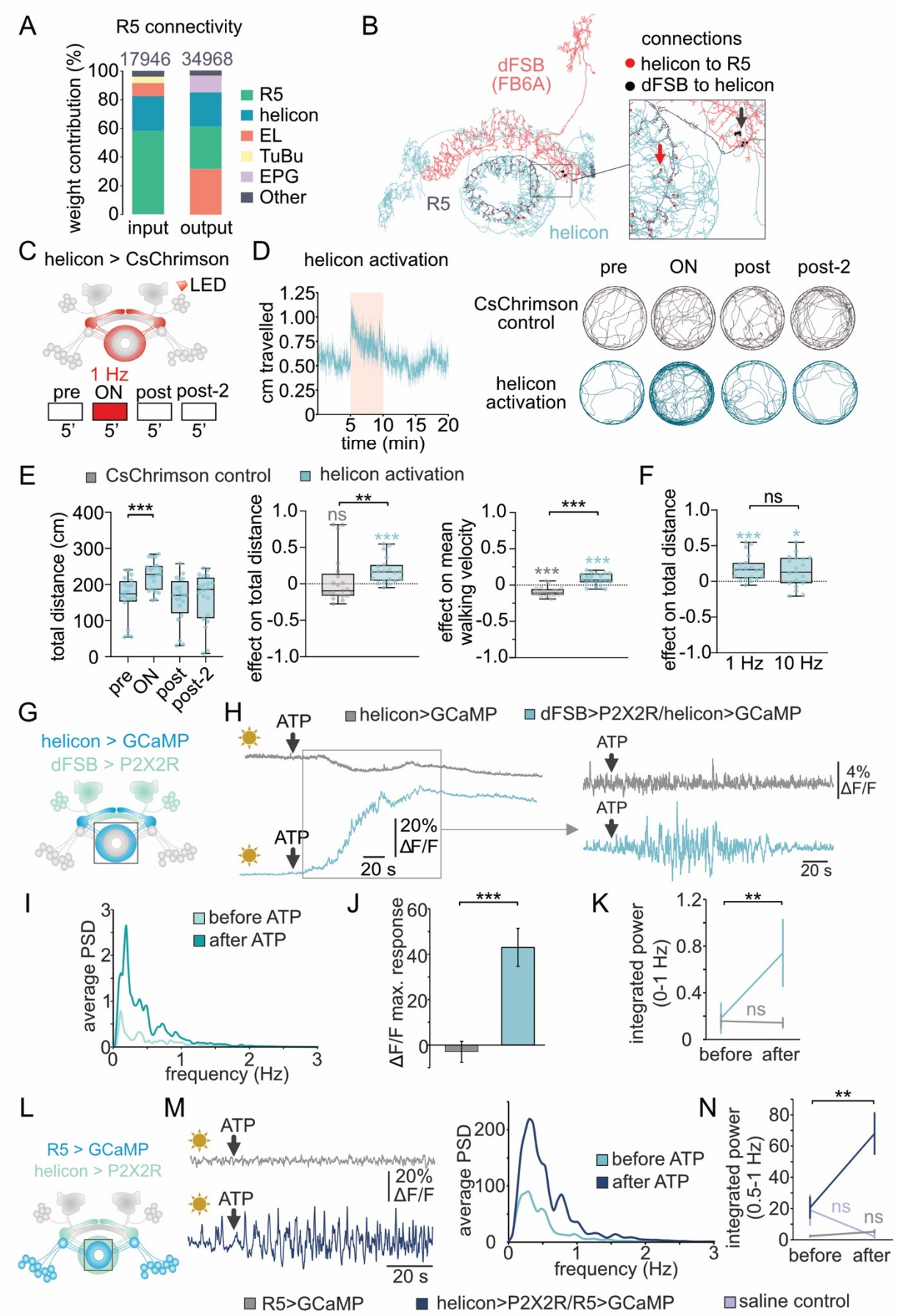
A
R5 connectivity
17946
34968
weight contribution (%)
input
output
R5
helicon
EL
TuBu
EPG
Other
B
dFSB
(FB6A)
R5
helicon
connections
helicon to R5
dFSB to helicon
C
helicon > CsChrimson
LED
1 Hz
pre
ON
post
post-2
5'
D
helicon activation
cm travelled
time (min)
pre
ON
post
post-2
CsChrimson control
helicon activation
E
CsChrimson control
helicon activation
total distance (cm)
effect on total distance
effect on mean walking velocity
F
effect on total distance
1 Hz
10 Hz
G
helicon > GCaMP
dFSB > P2X2R
H
ATP
helicon>GCaMP
dFSB>P2X2R/helicon>GCaMP
20%
ΔF/F
20 s
4%
ΔF/F
I
before ATP
after ATP
average PSD
frequency (Hz)
J
ΔF/F max. response
K
integrated power
(0-1 Hz)
before
after
L
R5 > GCaMP
helicon > P2X2R
M
ATP
20%
ΔF/F
20 s
average PSD
before ATP
after ATP
frequency (Hz)
N
integrated power
(0.5-1 Hz)
before
after
R5>GCaMP
helicon>P2X2R/R5>GCaMP
saline control

Figure 4. Oscillatory signatures in the locomotion-gating helicon network.
(A) Helicon cells connect to R5 and dFSB neurons and therefore could bridge sleep drive mediating neural circuits. Left: top synaptic input and output connections from R5 neurons indicate high connectivity with helicon cells. **(B)** Example circuit between a R5 neuron (body ID: 1200049187), helicon cell (body ID: 918334668) and dFSB neuron (FB6A) (body ID: 422191200). Red circles indicate areas of synaptic connections from the helicon cell to the R5 neuron and black circles areas of synaptic connections from the dFSB neuron to the helicon cell. Hemibrain connectome data was obtained using neuPrint (version 1.2.1). **(C)** Schematic overview of the optogenetic protocol used to activate helicon cells under 24B11-GAL4 control. **(D)** Left: average locomotion trace of 24B11-GAL4>UAS-CsChrimson (+ retinal), *n*=21 for CsChrimson control (+ retinal) and *n*=20 for helicon activation (+ retinal). Curves: mean ± SEM. Right: example trajectories of genotypes tested. **(E)** 1 Hz helicon stimulation increased distance travelled only during activation (panel 1), *n*=20, Friedman test with Dunn's multiple comparisons. Optogenetic stimulation increased total distance travelled and mean velocity of walking flies (panel 2 and 3) of 24B11-GAL4>UAS-CsChrimson flies compared to control flies, *n*=20-21 each group, Mann-Whitney test (comparisons between genotypes, black asterisks) and Wilcoxon signed-rank test (comparisons to baseline locomotion, colorful asterisks). Data of CsChrimson control flies was taken from **Fig. 3E** for comparison. **(F)** The effect of 1 Hz helicon stimulation on distance travelled did not differ between different frequencies of activation (*n*=20 for 1 Hz and *n*=19 for 10 Hz, Mann-Whitney test). **(G)** Schematic overview indicating ectopic expression of P2X2 receptors in dFSB and Ca^{2+} recording sites at the helicon ring. **(H)** Activation of dFSB increases presynaptic Ca^{2+} levels in the helicon network and induces a transient increase in oscillatory activity. Left: example traces of helicon Ca^{2+} activity (82F10-GAL4) after activation of dFSB neurons (23E10-LexA). Right: zoomed in and fitted traces reveal that dFSB activation can induce oscillatory activity in the helicon network. **(I)** Average power spectrum showing increased slow-wave power in helicon cells between 0-1 Hz after prolonged activation of dFSB neurons (*n*=12). **(J)** Absolute Ca^{2+} and **(K)** slow-wave power (0-1 Hz) is increased after dFSB activation (*n*=12, Mann-Whitney test for J, Wilcoxon matched-pairs signed rank test for K. **(L)** Schematic overview indicating ectopic expression of P2X2 receptors in helicon cells and Ca^{2+} recording sites at the presynaptic R5 ring. **(M)** Left: example traces of R5 presynaptic Ca^{2+} activity (88F06-GAL4) after prolonged activation of helicon cells (24B11-LexA). Right: average power spectrum (*n*=12) of R5 activity before and after application of ATP. **(N)** R5 slow-wave power (0.5-1 Hz) is increased after activation of helicon cells (*n*=7-12, Wilcoxon matched-pairs signed rank test). In all panels, significance is represented as follows: *$p \leq 0.05$ and **$p \leq 0.01$.

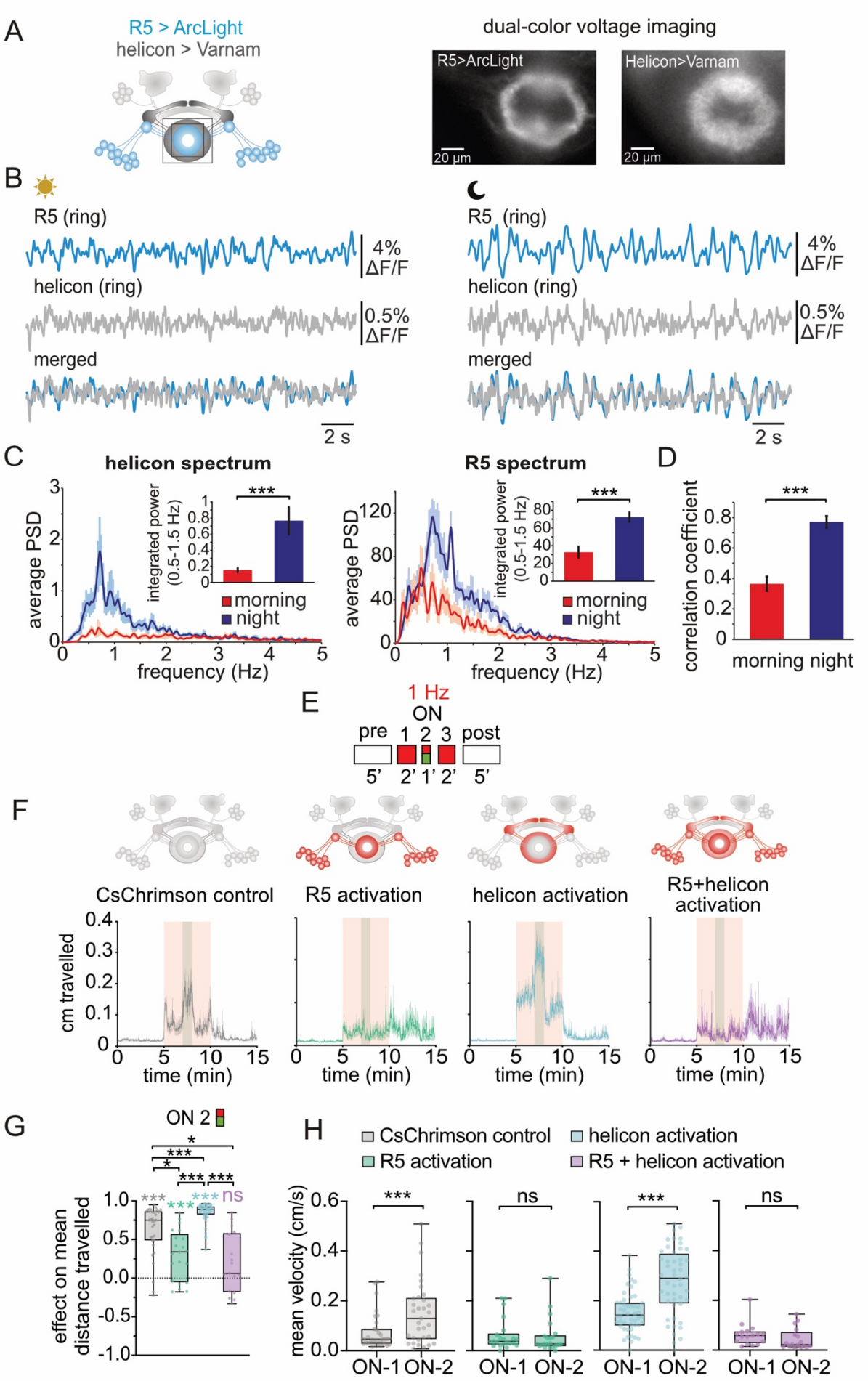
A
R5 > ArcLight
helicon > Varnam
dual-color voltage imaging
R5>ArcLight
Helicon>Varnam
20 µm
20 µm
B
R5 (ring)
helicon (ring)
merged
4% ΔF/F
0.5% ΔF/F
2 s
C
helicon spectrum
R5 spectrum
average PSD
frequency (Hz)
integrated power (0.5-1.5 Hz)
morning
night
***
D
correlation coefficient
morning night
E
1 Hz
ON
pre
1 2 3
post
5' 2' 1' 2' 5'
F
CsChrimson control
R5 activation
helicon activation
R5+helicon activation
cm travelled
time (min)
G
ON 2
effect on mean distance travelled
ns
H
CsChrimson control
helicon activation
R5 activation
R5 + helicon activation
mean velocity (cm/s)
ON-1 ON-2

Figure 5. Helicon and R5 networks synchronize oscillatory activity patterns at night to regulate arousal.

(A) Schematic and wide-field image of presynaptic ring structures expressing the green voltage indicator ArcLight in R5 neurons (88F06-GAL4) and the red voltage indicator Varnam in helicon cells (24B11-LexA). Squares indicate recording sites. **(B)** Example recordings of R5 and helicon presynaptic electrical patterns recorded in the morning (ZT 2-4) and at night (ZT 14-16). **(C)** Average power spectra of compound oscillations in R5 neurons and helicon cells demonstrate that slow-wave power (0.5-1.5 Hz) is increased at night in both networks (*n*=9-11 for helicon cells and R5 neurons, Mann-Whitney test). **(D)** Correlation between electrical patterns of helicon and R5 networks is significantly increased at night compared to the subjective morning (*n*=9-11, Mann-Whitney test). **(E)** Schematic overview of optogenetic activation protocol to test sensory processing during activation in sleeping flies. After 5 min of immobility, sleeping flies were presented with 5 min of 5-ms pulsed red light at 1 Hz and a continuous green light during the stimulation. **(F)** Average locomotion traces of CsChrimson control (+ retinal, *n=33*), 58H05-LexA>LexAop-CsChrimson (+ retinal, *n*=22), 24B11-LexA>LexAop-CsChrimson (+ retinal, *n=47*) and 58H05-LexA;24B11-LexA>LexAop-CsChrimson flies (+ retinal, *n=17)*. Curves: mean ± SEM. **(G)** Behavioral responsiveness to green light during optogenetic network activation (compared to baseline locomotion, colored asterisks). Behavioral responsiveness during R5 activation was reduced compared to helicon stimulation and control. Simultaneous activation of R5 of helicon led to the strongest impairment in behavioral responsiveness, *n*=17-47 each group, Kruskal-Wallis test with Dunn's multiple comparisons (black asterisks). **(H)** Behavioral responsiveness to green light (ON-2) compared to ON-1. Flies are only significantly aroused in the control and during helicon stimulation. R5 stimulations and simultaneous activation of R5+helicon inhibited arousal during visual stimulation, *n*=17-47 each group, Wilcoxon matched-pairs signed rank test. Behavioral data was taken during the subjective day of the flies (ZT 1-7) after a 12-19 h of sleep deprivation. In panels from **H-G**, box-plots show median (line), quartiles (boxes) and range (whiskers). In all panels, significance is represented as follows: *$p \leq 0.05$, **$p \leq 0.01$ and ***$p \leq 0.001$.

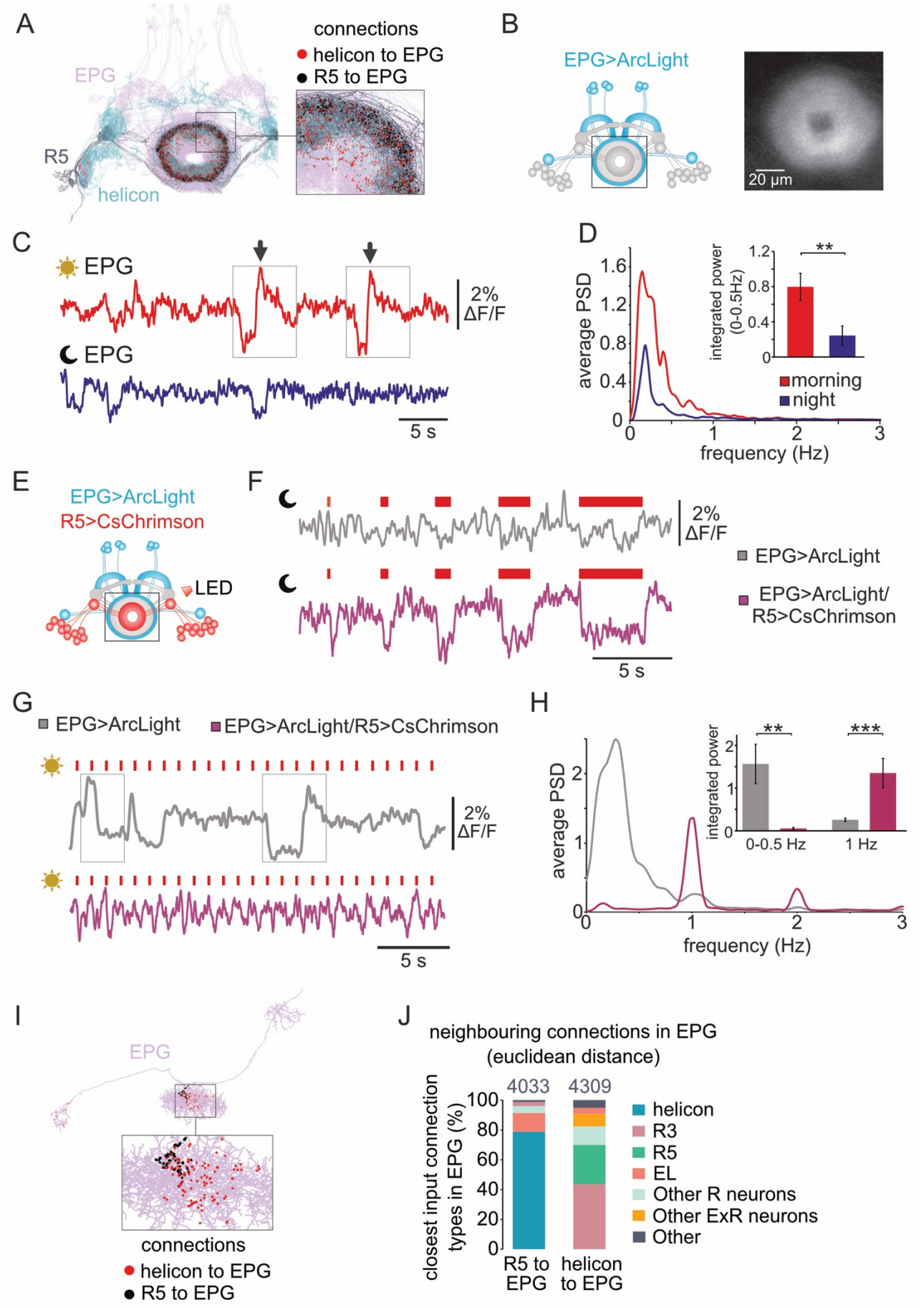
A
EPG
R5
helicon
connections
helicon to EPG
R5 to EPG
B
EPG>ArcLight
20 µm
C
EPG
EPG
2%
ΔF/F
5 s
D
average PSD
integrated power
(0-0.5Hz)
**
morning
night
frequency (Hz)
E
EPG>ArcLight
R5>CsChrimson
LED
F
2%
ΔF/F
5 s
EPG>ArcLight
EPG>ArcLight/
R5>CsChrimson
G
EPG>ArcLight
EPG>ArcLight/R5>CsChrimson
2%
ΔF/F
5 s
H
average PSD
integrated power
**
***
0-0.5 Hz
1 Hz
frequency (Hz)
I
EPG
connections
helicon to EPG
R5 to EPG
J
neighbouring connections in EPG
(euclidean distance)
closest input connection
types in EPG (%)
4033
4309
R5 to
EPG
helicon
to EPG
helicon
R3
R5
EL
Other R neurons
Other ExR neurons
Other

Figure 6: R5 network activity inhibits downstream head-direction neurons to suppress spontaneous activity.

(A) The helicon-R5-EPG circuitry strongly interconnects at the level of the ring. Morphological renderings of R5 neurons, helicon cells and EPG neurons. Red circles indicate areas of synaptic connections of helicon cells to EPG neurons and black circles areas of synaptic connections R5 to EPG. **(B)** Schematic and wide-field image of EPG neurons expressing the voltage indicator ArcLight (60D05-GAL4). **(C)** Example recordings of EPG electrical patterns recorded in the morning (ZT 2-4) and at night (ZT 14-16) indicating reduced activity at night. **(D)** Average power spectrum of EPG electrical activity demonstrates that spontaneous non-oscillatory events are markedly reduced at night (*n*=12, Mann-Whitney test). **(E)** Schematic overview of EPG recording site (60D05-GAL4) during optogenetic activation of R5 (58H05-LexA). **(F)** Example recordings showing that activation of R5 neurons hyperpolarize the EPG network. **(G)** Example recordings showing that 1 Hz activation of R5 neurons induces transient hyperpolarizations in EPG. **(H)** Average power spectrum of EPG electrical activity demonstrating that rhythmic activation of R5 neurons abolishes spontaneous events in the EPG network (0-0.5 Hz) while simultaneously generating peak activity at 1 Hz (*n*=8, Mann-Whitney test). **(I)** Location of R5 and helicon synapses projecting to a single EPG neuron (bodyId: 387364605). Red circles indicate areas of synaptic connections of helicon cells to EPG neurons and black circles areas of synaptic connections R5 to DPG. **(J)** Helicon to EPG synapses are found in proximity to R5 to EPG connections and other ring neuron to EPG synapses. Bar plots indicate the percentage of neighboring synapses of R5 to EPG and helicon to EPG connections per neuron type. For every R5 to EPG synaptic connection, the closest input synapse in the same EPG neuron excluding synapses from other R5 neurons is calculated based on Euclidean distance. Neighboring synapses of helicon to EPG connections excluding other helicon to EPG connections are calculated using the same procedure. Hemibrain connectome data was obtained using neuPrint (version 1.2.1). In all panels, significance is represented as follows: $^{**}p \leq 0.01$ and $^{***}p \leq 0.001$.

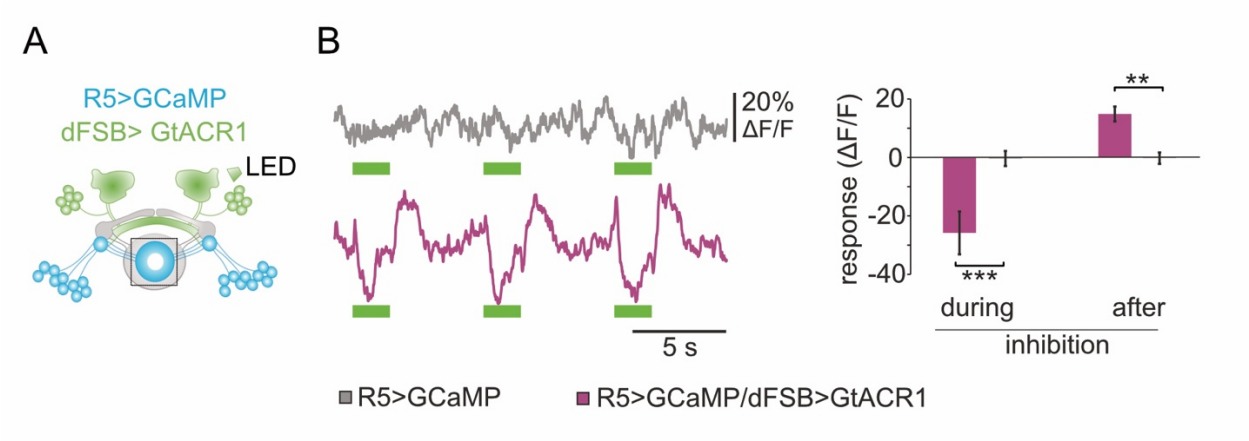

Figure S1. (A) Schematic overview indicating expression of GtACR1 in dFSB and Ca^{2+} recording sites at the R5 ring. **(B)** Left: average traces of R5 presynaptic activity (58H05-LexA) during optogenetic inhibition of dFSB neurons (*n*=3-4). Right: Inhibition of dFSB neurons leads to a transient reduction in R5 presynaptic Ca^{2+}. Release of Inhibition leads to a transient increase in R5 presynaptic Ca^{2+} (*n*=9-12, Mann-Whitney test). In all panels, significance is represented as follows: **$p \leq 0.01$ and ***$p \leq 0.001$.

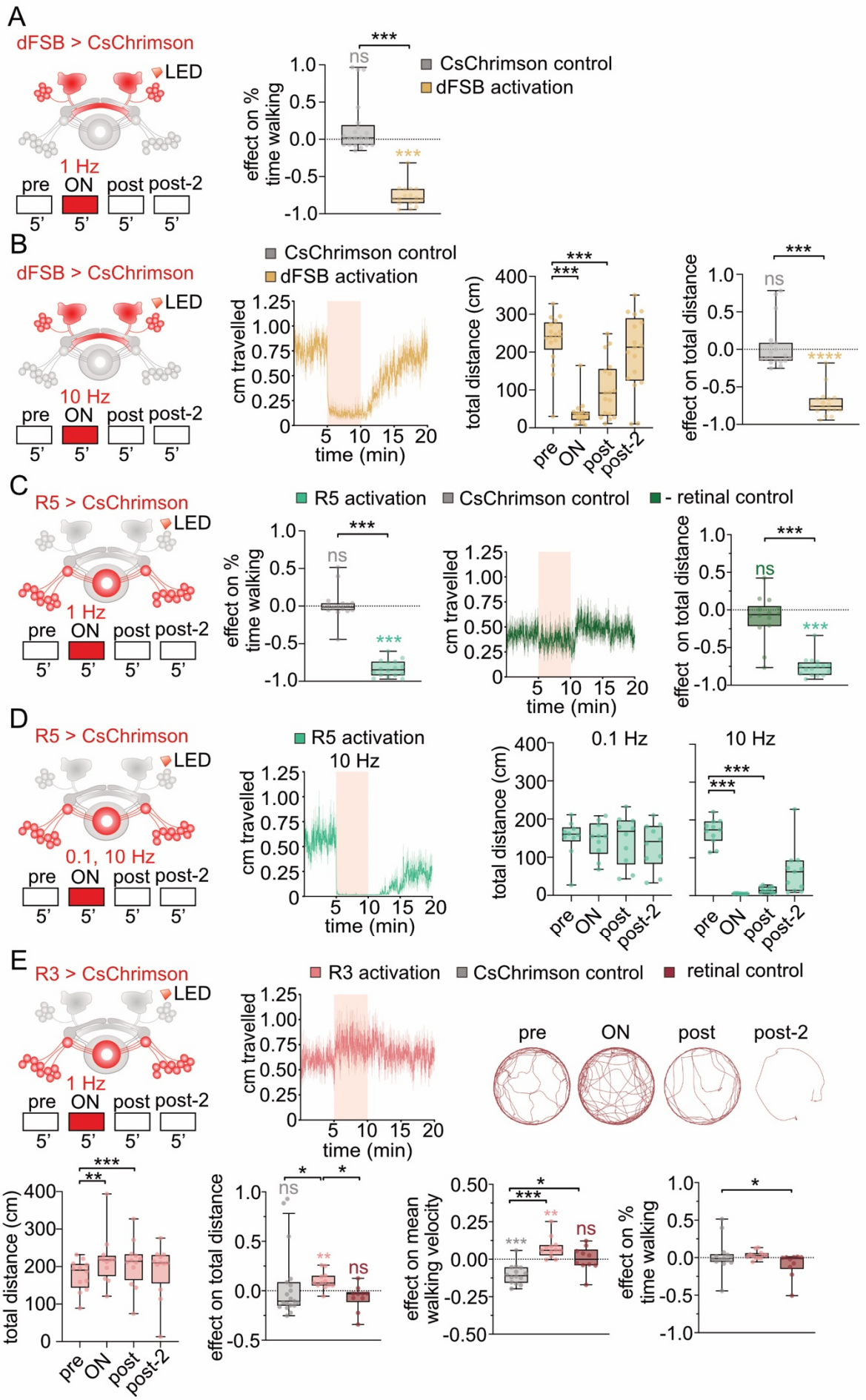
A
dFSB > CsChrimson
LED
1 Hz
pre ON post post-2
5' 5' 5' 5'
CsChrimson control
dFSB activation
effect on % time walking
B
dFSB > CsChrimson
10 Hz
cm travelled
time (min)
total distance (cm)
effect on total distance
C
R5 > CsChrimson
R5 activation
CsChrimson control
- retinal control
D
R5 > CsChrimson
0.1, 10 Hz
0.1 Hz
10 Hz
E
R3 > CsChrimson
R3 activation
CsChrimson control
retinal control
effect on mean walking velocity

Figure S2. (A) Optogenetic stimulation of dFSB neurons at 1 Hz in rested flies expressing CsChrimson under 23E10-GAL4 control decreased percentage of time walking compared to control flies, *n*=17-19 each group, Mann-Whitney test (comparisons between genotypes, black asterisks) and Wilcoxon signed-rank test (comparisons to baseline locomotion, colorful asterisks). **(B)** Optogenetic activation of dFSB at 10 Hz under 23E10-GAL4 control. Average locomotion traces of genotypes tested, *n*=19 for CsChrimson control (+ retinal) *n*=17 for dFSB activation (+ retinal). Curve: mean ± SEM. Activation of dFSB at 10 Hz decreased total distance travelled during and after activation, *n*=17, Friedman test with Dunn's multiple comparisons. The effect of activating dFSB at 10 Hz on distance travelled differed to that of control flies, *n*=17-19 each group, Mann-Whitney test (comparisons between genotypes, black asterisks) and Wilcoxon signed-rank test (comparisons to baseline locomotion, colorful asterisks). **(C)** Activation of R5 neurons at 1 Hz in rested flies expressing CsChrimson under 58H05-GAL4 control (+ retinal) decreased percentage of time walking compared to control flies, *n*=16 each group, Mann-Whitney test (comparisons between genotypes, black asterisks) and Wilcoxon signed-rank test (comparisons to baseline locomotion, colorful asterisks). Average locomotion trace of 58H05-GAL4>UAS-CsChrimson flies (- retinal), *n*=14. Curve: mean ± SEM. The effect of R5 activation at 1 Hz (+ retinal) differed to that of control flies (- retinal), *n*=12-16 each group, Mann-Whitney test (comparisons between genotypes, black asterisks) and Wilcoxon signed-rank test (comparisons to baseline locomotion, colorful asterisks). Data of retinal-fed flies was taken from **Fig. 3J** for comparison. **(D)** Activation of R5 neurons at different frequencies in rested flies expressing CsChrimson under R58H05-GAL4 control. Average locomotion trace of 58H05-GAL4>UAS-CsChrimson flies (+ retinal) exposed to 10 Hz (*n*=9) red light pulses. Curve: mean ± SEM. **(G)** Activation of R5 neurons in rested flies at 0.1 Hz did not affect locomotion, whereas 10 Hz stimulation reduced distance travelled during and after activation, *n*=9-10 each group, Friedman tests with Dunn's multiple comparisons. **(E)** Activation of R3 ring neurons at 1 Hz in rested flies expressing CsChrimson under 84H09-GAL4 control. Average locomotion trace of 84H09-GAL4>UAS-CsChrimson flies (+ retinal), *n*=12. Curve: mean ± SEM. Example trajectories of genotypes tested. Activation of R3 neurons in rested flies increased distance travelled during and after activation, *n*=12, Friedman test with Dunn's multiple comparisons. The effect of activating R3 on distance travelled, velocity of walking flies and percentage of time walking differed to that of genetic and retinal controls, *n*=14 for CsChrimson control (+ retinal), *n*=10 for (-) retinal control and *n*=13 for R3 activation, Kruskal-Wallis test with Dunn's multiple comparisons. Data of CsChrimson control flies was taken from **Fig. 3I** for comparison. Experiments shown in this figure were done during the subjective day of the flies (ZT 1-10). In all panels, box-plots show median (line), quartiles (boxes) and range (whiskers) and significance is represented as follows: *$p \leq 0.05$, **$p \leq 0.01$ and ***$p \leq 0.001$.

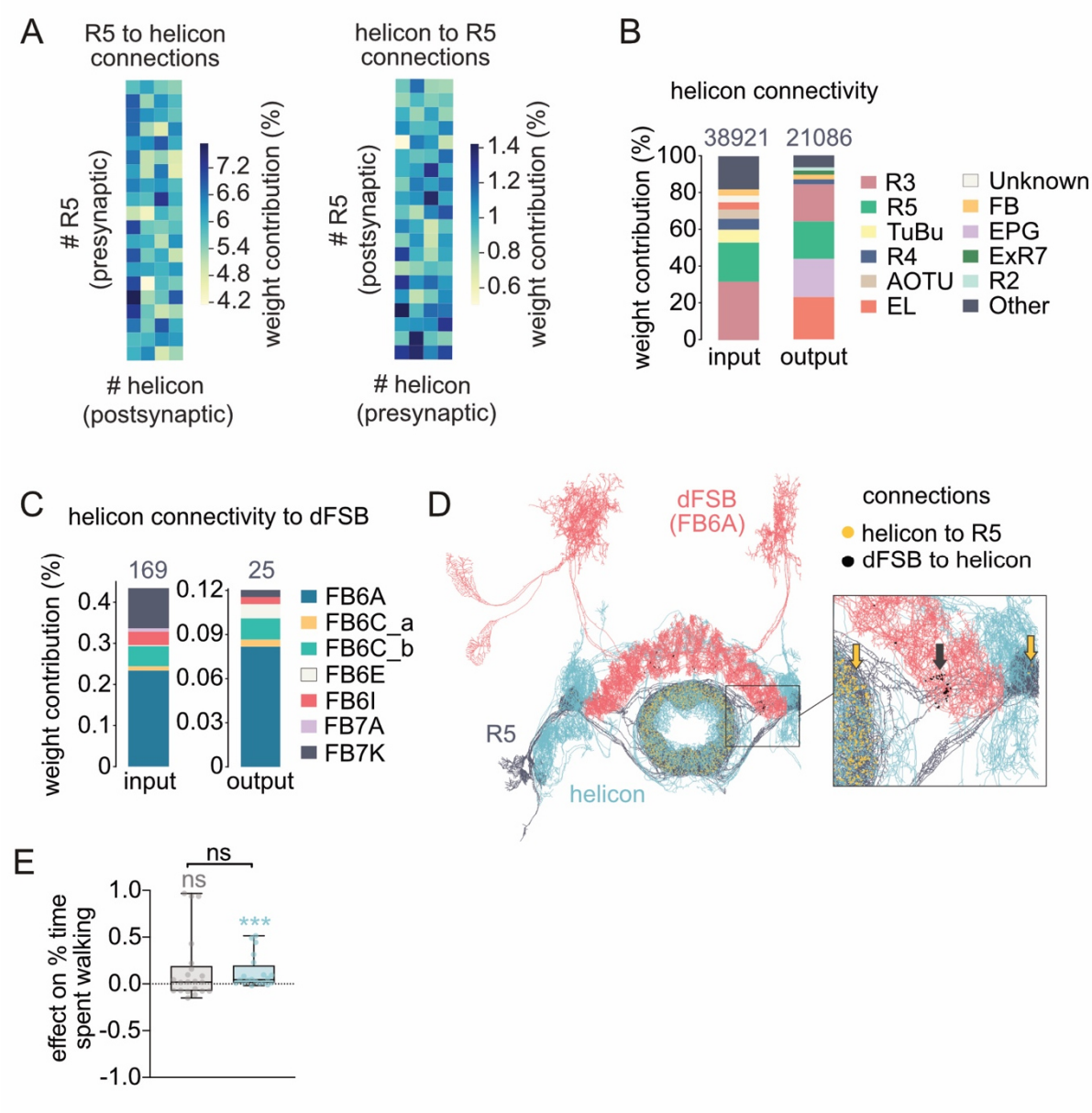

Figure S3. (A) Neuron-to-neuron connectivity plot for connections from R5 neurons to helicon cells (left) and from helicon cells to R5 neurons (right). Number of connections are normalized to the total number of output connections of each R5 neuron (left) and to the total number of output connections of each helicon cell (right). **(B)** Top synaptic input and output connections of all helicon cells. **(C)** Fraction of helicon cell input and output from dFSB layers normalized to the total number of input and output connections of helicon cells. **(D)** Morphological renderings of R5 neurons, helicon cell and FB6A (dFSB) neurons. Yellow circles indicate areas of synaptic connections of helicon cells to R5 neurons and black circles areas of synaptic connections dFSB to helicon. **(E)** Optogenetic stimulation of helicon cells at 1 Hz in rested flies expressing CsChrimson under 24B11-GAL4 control decreased percentage of time walking compared to control flies, *n*=20-21 each group, Mann-Whitney test (comparisons between genotypes, black asterisks) and Wilcoxon signed-rank test (comparisons to baseline locomotion, colorful asterisks), ***$p \leq 0.001$.

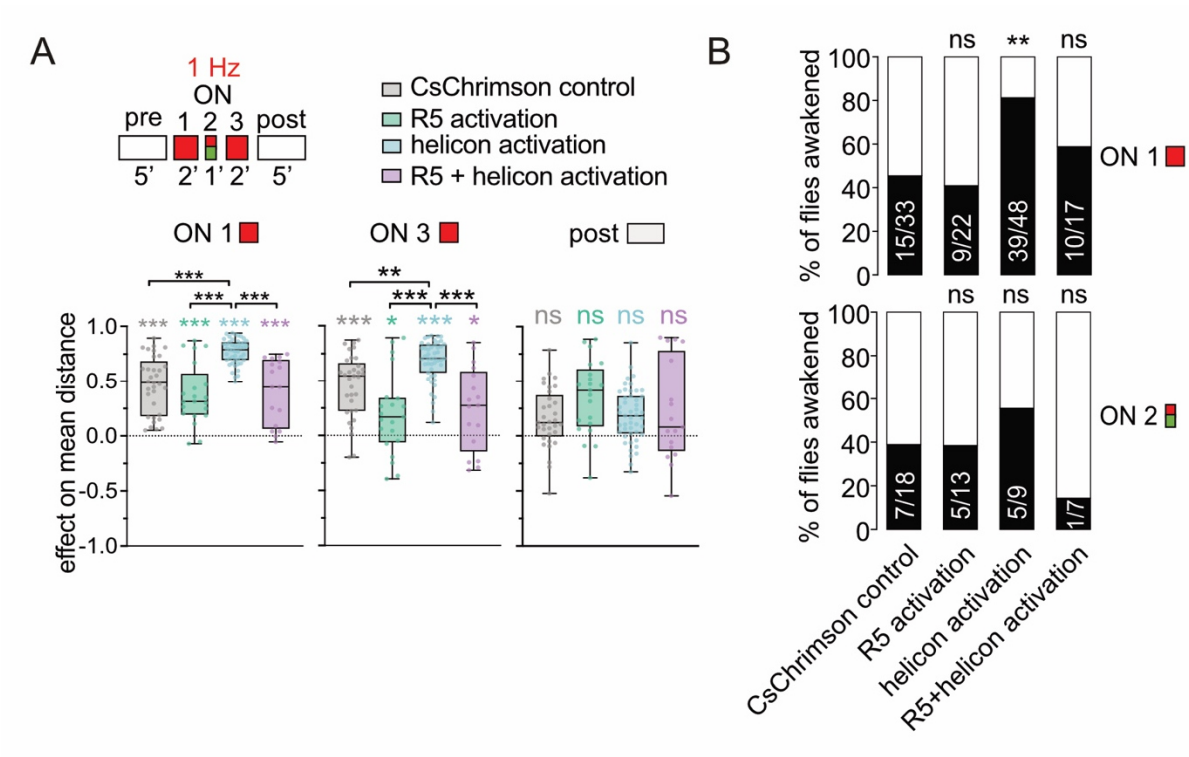

Figure S4. (A) Schematic overview of optogenetic activation protocol to test visual responsiveness during network activation in sleep deprived flies (described in **Fig. 5E**). Effect of optogenetic and arousal protocol on mean distance travelled at different times of the experiment (ON1: during activation, before green light; ON3: during activation, after green light; post: after activation, after light). The effect of helicon activation on locomotion differed to that of R5 and R5+helicon activation, *n=33* for CsChrimson control, *n*=22 for 58H05-LexA>LexAop-CsChrimson, *n*=47 for 24B11-LexA>LexAop-CsChrimson and *n*=17 for 58H05-LexA;24B11-LexA>LexAop-CsChrimson, Kruskal-Wallis test with Dunn's multiple comparisons (comparisons between genotypes, black asterisks) and Wilcoxon signed-rank tests (comparisons to baseline locomotion, colorful asterisks). Box-plots show median (line), quartiles (boxes) and range (whiskers). Behavioral data was taken during the subjective day of the flies (ZT 1-7) after 12-19 h of sleep deprivation. **(B)** Percentage of sleeping flies that started walking ('awakened') at the beginning of the optogenetic stimulation (top, 'ON 1') or when exposed to green light (bottom, 'ON' 2). 1 Hz stimulation of the helicon network led to more flies waking up at the beginning of the stimulation when compared to the genetic control, Binomial test. The *n* of flies for each condition is indicated in the bar plots. In all panels, significance is represented as follows: *p ≤ 0.05, **p ≤ 0.01 and ***p ≤ 0.001.